


A comparative study of cartilage engineered constructs in immunocompromised, humanized and immunocompetent mice

Journal Article**Author(s):**

Cavalli, Emma; Fisch, Philipp; Formica, Florian A.; Gareus, Ralph; Linder, Thomas; Applegate, Lee Ann; [Zenobi-Wong, Marcy](#) 

Publication date:

2018-09

Permanent link:

<https://doi.org/10.3929/ethz-b-000304832>

Rights / license:

[Creative Commons Attribution-NonCommercial-NoDerivatives 4.0 International](#)

Originally published in:

Journal of Immunology and Regenerative Medicine 2, <https://doi.org/10.1016/j.regen.2018.09.001>

1 **A comparative study of cartilage engineered constructs in**
2 **immunocompromised, humanized and immunocompetent**
3 **mice**

4 Emma Cavalli^{1,†}, Philipp Fisch^{1,†}, Florian A. Formica¹, Ralph Gareus², Thomas Linder³,
5 Lee Ann Applegate⁴, Marcy Zenobi-Wong^{1,§}

6 ¹ Tissue Engineering and Biofabrication, Institute for Biomechanics, Swiss Federal
7 Institute of Technology Zürich (ETH Zürich), Otto-Stern-Weg 7, 8093 Zürich, Switzerland

8 ² The Jackson laboratory, 600 Main St, Bar Harbor, ME 04609, USA

9 ³ Department of Otorhinolaryngology, Head- & Neck Surgery, Luzerner Kantonsspital,
10 Spitalstrasse, 6000 Luzern, Switzerland

11 ⁴ Department of Musculoskeletal Medicine, Regenerative Therapy Unit, University
12 Hospital of Lausanne (CHUV), EPCR/ch. Croisettes 22, 1066 Epalinges, Switzerland

13 †These authors contributed equally to this study

14 § Address for correspondence:

15 Prof. Marcy Zenobi-Wong

16 ETH Zürich

17 Tissue Engineering and Biofabrication

18 HPL J22

19 Otto-Stern-Weg 7

20 8093 Zürich, Switzerland

21 zmarcy@ethz.ch

22 Phone: +41 44 632 5089

23 **Keywords:** chondroprogenitors, auricular chondrocytes, biomaterial, hyaluronic acid

24

25 **Highlights**

26 • Chondrogenesis of a tissue-engineered cartilage graft is feasible in
27 immunocompetent small animals

28 • Immunocompetent and immunodeficient animals lead to analogous results in
29 terms of chondrogenesis, as long as the implanted cells are shielded from the host
30 by a biomaterial

31 • Subcutaneous implantation in small animals with a complete and human immune
32 system could help to predict the outcome of engineered grafts for cartilage
33 applications

34

35 **Abstract**

36 Choosing the best ectopic *in vivo* model for cartilage engineering studies remains
37 challenging and there is no clear consensus on how different models compare to one
38 another. The use of xenogenic cells can often limit the choice to immunocompromised
39 animals only and thus prevents the understanding of how tissue-engineered grafts
40 perform with potential active inflammatory and immunological responses. The aim of this
41 study was to evaluate the chondrogenic potential of a recently developed hydrogel,
42 hyaluronan transglutaminase (HA-TG), in four mouse strains with varying immune
43 systems: NSG, nude, NSG-SGM3 humanized and C57BL/6. The hyaluronan-based hydrogel

44 was implanted subcutaneously for 4 weeks after an *in vitro* pre-culture time of 4 weeks.
45 Scaffolds were prepared without cell seeding as the control and in combination with
46 either human auricular chondrocytes (hAUR) or human fetal chondroprogenitor cells
47 (hCC). We have seen that constructs were able to maintain their volumes and resisted
48 vascularization as well as macrophage infiltration *in vivo*. Both hAUR and hCC maintained
49 and produced ECM *in vivo*, but hAUR showed higher levels of innate collagen 2 even
50 without mechanical stimulation. Collagen 1 and 2 deposition as well as mechanical
51 properties of the scaffolds were comparable in all mouse strains. The C57BL/6 mouse
52 model consistently displayed higher levels of C-reactive protein (CRP), serum amyloid A
53 (SAA), and serum amyloid protein (SAP) in serum as a reaction to the foreign material and
54 human cells. In addition, the number of CD68+ and CD163+ macrophages as well as CD3+
55 lymphocytes around the constructs in C57BL/6 mice was significantly higher than in
56 humanized and immunocompromised mouse models. The results show that it is possible
57 to engineer a cartilage-like graft subcutaneously not only in immunocompromised, but
58 also in immunocompetent and humanized mouse model.

59

60 **1. Introduction**

61

62 *In vivo* testing plays a key role in tissue engineering and in providing the pre-clinical data
63 necessary to bring new therapies to the clinic [1]. Despite recent advances with *in vitro*
64 techniques such as bioreactors, organ-on-a-chip and organoids, animal models remain
65 critical, particularly for safety assessment of tissue engineering components. This is no
66 exception in the cartilage repair field where animal models continue to be required for
67 regulatory approval of biologics and devices [2]. Nevertheless, choosing the appropriate
68 animal model for the assessment of new cellular-, drug- or biomaterial-based strategies
69 for cartilage repair remains a major challenge. Animal type, size and physiological
70 differences inter- and intra-species can have a significant influence on the outcome of a
71 study. Additionally, the limited ability of cartilage to regenerate has driven the
72 development of cell-based and tissue engineering techniques [3] which often involve the
73 use of allogenic cells [4-6] and allografts [7-9]. The widespread use of
74 immunocompromised mice for preclinical studies often prevents a full understanding of
75 how tissue-engineered constructs perform in terms of chondrogenesis and inflammatory
76 response when exposed to an active immune system.

77 Under current regulatory scrutiny, a number of aspects need to be kept in consideration
78 when choosing the animal model for cartilage tissue engineering. Despite the value of
79 large animal models, there are still ethical, economical and technical constraints that
80 prevent their wide-spread utilization and acceptance [1]. Furthermore, despite the recent
81 advances in gene-editing techniques like CRISPR-Cas9, the availability of transgenic
82 models in large animals is still limited [10]. Rodents, and particularly mice, are affordable,
83 easy to manage and can provide proof-of-concept data in a time-effective manner. They

84 can be genetically modified to insert and delete specific genes and they are commercially
85 available in a variety of athymic, transgenic and knockout strains. Therefore they are
86 usually a first choice in cartilage engineering studies for screening purposes and to bridge
87 the gap between *in vitro* experiments and large animal preclinical studies [11].

88 Chondrogenesis for cartilage engineering strategies has been extensively studied in
89 murine models by subcutaneous implantations. The subcutaneous implant model was
90 developed due to the limited joint size and cartilage thickness of mice [11, 12] and allows
91 the evaluation of tissue-engineered constructs to sustain and induce cartilage formation
92 in an ectopic site as well as the ability of the construct to resist cellular infiltration.

93 Athymic nude mice, which have a limited adaptive immune response, are the most
94 commonly used strain of mice in cartilage engineering [12]. They are hairless and their
95 lack of the thymus prevents them from having a cell-mediated immunity [13]. Indeed in
96 nude mice, the immune response to foreign and xenogeneic bodies
97 does not involve the activation of antigen-specific T lymphocytes and the consequent release
98 of cytokines. Another widely-used mouse strain is the NOD (non-obese diabetic) SCID
99 (severe combined immunodeficiency) gamma, or NSG. NSG mice are among the most
100 immunodeficient mouse strain described to date, lack mature T cells, B cells, and natural
101 killer (NK) cells and have a defective innate immune system [14].

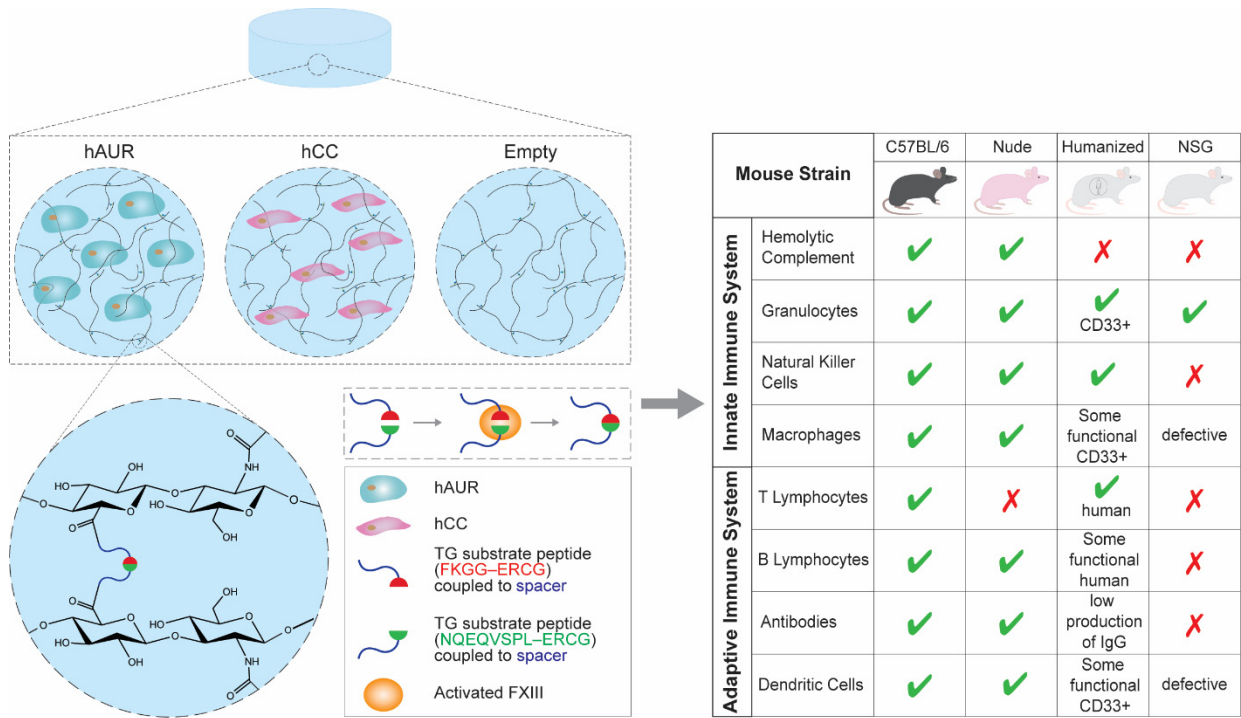
102 In the attempt to reduce the gap between pre-clinical and clinical studies, mouse-human
103 chimeras, or humanized mice, have been developed [15]. Humanized mice are
104 immunodeficient mice engrafted with human hematopoietic cells or human peripheral-
105 blood mononuclear cells. Of these mice, the NSGTM-SGM3 transgenic strain contains three
106 co-injected human transgenes, the Stem Cell Factor (SCF), the Granulocyte/Macrophage
107 colony factor 2 (GM-CSF) and the interleukin-3 (IL-3). Thanks to this triple transgenic
108 modification, NSGTM-SGM3 mice constitutively express cell proliferation and survival

109 signals and support a stable engraftment of human hematopoietic cells. This strain is
110 gaining popularity in the immune-oncology field to understand the interactions between
111 human immune cells and specific patient-derived tumors due to its high count of human
112 immune cell populations (i.e. CD19+ B cells, CD3+ T cells, CD33+ myeloid cells) [16-18].
113 Additionally, they have proven to be a very valuable tool in the study of the human
114 immune system development and dysfunction as well as in the modelling of several
115 human diseases (e.g. infectious diseases such as Epstein Barr virus infection and HIV, and
116 autoimmune diseases such as diabetes and arthritis) with minor logistical and ethical
117 concerns [19]. Nevertheless, current humanized mice lack secondary lymphoid tissue and
118 can only partially mimic the complexity of a fully developed, human immune system,
119 which is the coordinated response of stromal, lymphoid, myeloid and secondary lymphoid
120 structures. Furthermore, the remaining murine immune system prevents the complete
121 human engraftment and murine cytokines do not fully support human myeloid and
122 lymphoid development [20, 21]. While effort are currently undergoing to overcome these
123 limitations, it is still an open question whether humanized mice could be used in the tissue
124 engineering field and represent a useful model in the preclinical study of tissue-
125 engineered graft transplantation.

126 Despite the widespread use of immunodeficient mice for the subcutaneous implantation
127 of engineered constructs for cartilage repair applications, there is no consensus as to
128 whether this should be the ideal choice for a mouse model. The recent development of
129 humanized mice has furthermore raised the question of whether these chimeras would
130 represent a suitable animal model for the field.

131 The aim of this study was to evaluate and compare the chondrogenic potential of a
132 recently developed tissue engineered scaffold for cartilage repair applications in four

133 different mouse strains, namely NSG, nude, NSG-SGM3 humanized and C57BL/6. The
134 biomaterial used was a hyaluronan-based hydrogel [22, 23], produced by functionalizing
135 the hyaluronan (HA) backbone with transglutaminase (TG) crosslinkable peptides,
136 hereby addressed as HA-TG. The material was investigated alone and in combination with
137 one of two cell types of different origins: human auricular chondrocytes (hAUR) and
138 human fetal chondroprogenitor cells (hCCs) (*Figure 1*). We investigated how differences in
139 the innate and adaptive immune systems of the mouse strain affect the quality and
140 amount of extracellular matrix (ECM) produced and maintained by the cells. hCCs are a
141 newly proposed cell source [24], which have previously shown to produce phenotypically
142 stable cartilage in combination with HA-TG *in vitro* [22] and in different collagen scaffolds
143 in an *in vivo* subcutaneous mouse model [25]. Allogeneic cells derived from fetal or
144 juvenile tissue have the additional benefit of not only having a more stable phenotype and
145 higher chondrogenic potential than adult articular chondrocytes [26], but also lower
146 immunogenicity [27]. Fetal chondroprogenitors have high stability and therefore very
147 large quantities of cells may be prepared from one, single organ donation allowing for the
148 development of Master and Working Cell banks (MCB & WCB). These cell banks provide
149 a long-term solution as the cells can be thawed just before use in transplantation.
150 Alternatively, auricular chondrocytes are currently emerging as a potential autologous
151 cell source for tissue engineering purposes due to their ease in harvesting from the
152 patient, enhanced proliferation capacity, high and reproducible chondrogenic potential
153 after *in vitro* expansion and the quality of the generated tissue [28]. Importantly, auricular
154 chondrocytes can be obtained from a cartilage biopsy with minimal donor site morbidity
155 compared to articular cartilage sites and therefore are suitable for autologous
156 applications in a clinical setting.



157

158 *Figure 1 Schematics of the study. Cell-laden (either human auricular chondrocytes, hAUR or human fetal*
 159 *chondroprogenitors, hCCs) and acellular hyaluronic acid-transglutaminase (HA-TG) hydrogels were prepared. HA-TG*
 160 *synthesis was achieved by functionalizing the side chains of a hyaluronan backbone with transglutaminase (TG) substrate*
 161 *peptides coupled to a spacer. Gelation occurred via crosslinking of the two TG peptides and was triggered by addition of*
 162 *activated factor XIII (FXIII) in presence of calcium. The constructs were subcutaneously implanted in four mouse strains*
 163 *with varying immune systems: NSG, nude, NSG-SGM3 and C57B6/6.*

164

165 **Materials and Methods**

166 **2.1 Chemicals**

167 All chemicals were purchased from Sigma-Aldrich unless stated otherwise.

168 **2.2 Cell sources**

169 Human hCCs were isolated from the proximal ulnar epiphysis of a 14 week gestation
170 organ donation (same donor as used in Darwiche *et al.* [24] and Studer *et al.* [25], Centre
171 Hospitalier Universitaire Vaudois, Ethics Committee Protocol No. 62/07) and registered
172 under the Federal Transplantation Program complying with the associated laws, Biobank
173 procedures and regulations.

174 Human auricular chondrocytes (male, 17 years old) were isolated from auricular cartilage
175 of otoplasty patients after having received informed consent (BASEC-Nr.2017-02101).

176 **2.3 Cell isolation, culture and expansion**

177 • hCC. The biopsy was collected and processed as previously described [24] except
178 that Trypsin/EDTA (Thermo Fisher Scientific) was used during processing to
179 prepare more uniform populations from the tissue and no antibiotics were used
180 for cell culture to develop the MCB. A WCB was developed for the project that was
181 derived from the MCB from the organ donation to provide equivalent cells
182 throughout the current project. The cells were expanded to passage 4 in Dulbecco's
183 modified Eagle's medium (DMEM; Gibco) containing 10% v/v FBS (Gibco), 2 mM
184 L-glutamine (Gibco) and 10 µg/ml Gentamycin (Gibco).

185 • hAUR. The cartilage pieces were washed extensively with PBS containing 50 µg/ml
186 gentamicin and incubated in 0.5% w/v pronase solution for 1.5 hour. The cartilage
187 was then minced into pieces of 1-3 mm³ and digested in 0.12% w/v collagenase
188 solution (DMEM, 12 mg/ml collagenase from *Clostridium histolyticum*, 10% v/v
189 FBS) overnight with gentle stirring at 30°C. The resulting cell suspension was
190 passed through a 40 µm cell strainer before collecting the cell pellet by
191 centrifugation (500 rcf for 10 minutes). The cells were plated at 10'000 cells/cm²
192 and expanded to passage 2 in DMEM, 10% v/v FBS, 10 µg/ml gentamycin and 50
193 µg/ml L-ascorbate-2-phosphate at 37°C, 5% CO₂ and 95% humidity.

194 ***2.4 HA-TG synthesis and hydrogel formation***

195 • HA-TG synthesis. HA-TG hydrogel precursors were synthesized as described
196 previously by Broguiere *et al.* [23]. Briefly, 400 mg of HA sodium salt (Lifecore
197 Biomedical, 1.01-1.8 MDa), and 23.8 mg of 3,3'-Dithiobis(propanoic dihydrazide)
198 (Frontier Scientific) were dissolved in 160ml of 150mM MES solution. Thereafter
199 38.4 mg of 1-Ethyl-3-(3-dimethylaminopropyl)carbodiimide (Fluka) was added
200 dropwise and left to react overnight. 143.33 mg of TCEP-HCl (Fluorochem) was
201 added, and the reduction left to proceed overnight. The product was dialyzed
202 against ultrapure water balanced to pH 4.5. The recovered solution was added
203 dropwise into a solution of 1 ml divinyl sulfone (DVS) in 40 ml of 300mM
204 triethanolamine (TEOA) buffer, pH 8.0. The reaction was left to proceed for 8h at
205 RT and then dialyzed against ultrapure water to yield vinyl sulfone-substituted HA
206 (HA-VS). The recovered HA-VS was split in two equal parts. One half was
207 functionalized with a substrate peptide that provided a reactive glutamine residue
208 (TG/Gln: NQEQVSPL-ERCG) and the other half with the peptide providing the

209 reactive lysine (TG/Lys: FKGG-ERCG). For conjugation, 10 ml of TEOA buffer 300
210 mM, pH 8.0 was added to each HA-VS portion and the peptides were added at 1.3
211 excess over the 10% DVS substitution. The reactions were allowed to proceed
212 overnight without stirring. Finally, the products were dialyzed against ultrapure
213 water, sterilized by 0.4 μ m filtration, lyophilized and stored at -80°C until use.

214 • Cell encapsulation. Cells (either hCC or hAUR) were suspended at a concentration
215 of 15 million cells/ml in HA-TG. The gelation was triggered as described by
216 Broguiere & Cavalli *et al.* [22]. Briefly, the gel precursors were resuspended at 2%
217 w/v in sterile filtered TBS (NaCl 150mM, CaCl₂ 50 mM, TRIS 50 mM, balanced to
218 pH 7.6). The crosslinking was initiated by adding thrombin (Baxter) and factor XIII
219 (Fibrogammin, CSL Behring) to a final concentration of 12.5U/ml and 10U/ml
220 respectively. The gels were quickly cast in UV-sterilized PDMS cylindrical molds
221 (SYLGARD 184, Corning, diameter=4mm, height= 2mm) adhered to 10 mm glass
222 coverslips. The gels were allowed to crosslink for 15 minutes at 37°C before adding
223 chondrogenic medium, consisting of high glucose DMEM supplemented with 10
224 ng/ml transforming growth factor β 3 (TGF- β 3, Peprotech), 50 μ g/ml L-ascorbate-
225 2-phosphate, 40 μ g/ml L-proline, 0.5% penicillin-streptomycin (Gibco) and 1%
226 ITS+ Premix (Corning). The PDMS molds were then detached from the cover slip
227 and the gels left free floating.

228 Gels without encapsulated cells were prepared as well and used as controls. The
229 cultures were maintained for up to 8 weeks, replacing the medium 3 times a week.

230 **2.5 Subcutaneous implantation**

231 Animal studies were performed in compliance with the ethical license (Application No.
232 ZH189/2014). Nude (Crl:NU(NCr)-Foxn1nu) and Black 6 (Crl:C57BL/6J), indicated in the
233 figures as Bl6) animals were obtained from Charles River, while NOD scid gamma (NSG)
234 and CD34+ humanized (NSG-SGM3, indicated in the figures as hu-NSG) mice were
235 obtained from The Jackson Laboratory. All animals were female with an age of 2-3 months
236 and a weight of 23 g \pm 4g. NSG-SGM3 animals were engrafted using fetal CD34+ cord blood
237 cells purchased from Lonza (as the Certificate of Analysis states “The cells were isolated
238 from donated human tissue after obtaining permission for their use in research
239 applications by informed consent or legal authorization”, Lot N. 0000625909). The
240 animals were used 18 weeks post engraftment, when the highest number of myeloid cells
241 was present (*Supplementary Table 1*). Animals were housed in groups of 4-5 and allowed
242 to move without restrictions. Standard food and water were provided *ad libitum*.

243 Different conditions were investigated during the study: HA-TG alone (acellular), HA-TG
244 with hCC and HA-TG with hAUR. Following randomization, six scaffolds of each condition
245 were subcutaneously implanted after 4 weeks of preculture in four different mouse
246 strains: C57BL/6, nude, NSG and NSG-SGM3. Six constructs per condition were further
247 cultured *in vitro*. Three animals were used for each experimental condition, for a total of
248 9 mice per strain. Mice were anesthetized with 4.5% isoflurane and Meloxicam
249 (Metacam, 2 mg/kg) was administered via subcutaneous injection before surgery. Eye
250 cream was applied to prevent desiccation of the cornea and the anesthesia was continued
251 with 1.5-3% isoflurane. Two incisions were made in the skin lateral to the dorsal midline
252 at the level of the hip joint and constructs were placed subcutaneously. The incisions were
253 closed with surgical staples (3M), which were removed after 1 week. Blood samples were

254 collected 10 days before surgery through puncture of the Vena Saphena and at the end of
255 all procedures and experimentation via heart puncture. After 4 weeks, the animals were
256 euthanized via CO₂ asphyxiation and the explants fixed for 2 hours in 4%
257 paraformaldehyde.

258 **2.6 Histology and immunohistochemistry**

259 After dehydration, samples were paraffin embedded and 5 µm sections were cut using a
260 microtome. Collagen 1 and 2 staining were performed after 30 minutes of 0.2% (w/v)
261 hyaluronidase digestion at 37 °C and 1 hour blocking with 5% normal goat serum (NGS)
262 with 1:1500 diluted rabbit anti-collagen 1 (Abcam ab138492) and 1:200 diluted rabbit
263 anti-collagen 2 (Rockland 600-401-104) antibodies. CD68, CD163 and CD3 stainings
264 were performed after heat-mediated epitope retrieval in sodium citrate buffer at pH 6 for
265 20 minutes, permeabilization in 0.3% v/v Triton-X for 15 minutes and 1 hour blocking
266 with 5% NGS with 1:200 diluted rabbit anti-CD68 (Abcam ab125212), 1:200 anti-CD163
267 (Abcam ab182422) and 1:100 anti-CD3 (Abcam ab5690) antibody respectively. Negative
268 controls were performed using a rabbit IgG isotype control (Novus Biologicals, NBP2-
269 24891) diluted 1:200.

270 All primary antibodies were diluted in 1% w/v NGS in PBS and incubated overnight at
271 4°C. Alexa Fluor 594 Goat Anti-Mouse IgG (Thermo Fisher Scientific, A11005) and Alexa
272 Fluor 488 Goat anti-rabbit Alexa 488 (Thermo Fisher Scientific, A11008) secondary
273 antibodies were used at 1:200 dilution in 1% NGS in PBS for 1 hour at RT. Finally, the
274 slides were incubated for 15 minutes with the nuclear stain DAPI (Molecular Probes) and
275 mounted with VectaMount AQ Mounting Medium (Vector Laboratories).

276 Safrainin O/Fast Green and hematoxylin and eosin (H&E) staining were performed using
277 standard protocols.

278 All of the images in the same figure were acquired using an automated digital slide scanner
279 (Panoramic 250 Flash III, 3D Histotech) using the same exposure time and light intensity.

280 For semi-quantitative analysis of collagen 1 and 2, the 8-bit integrated density of the
281 stainings were analyzed using ImageJ v1.51 software (National Institutes of Health). For
282 quantification analysis of CD68 and CD163, positively stained cells were counted in
283 randomly selected regions of interest in the fibrous capsule around the scaffolds and
284 expressed as the mean number of cells per region of interest (cells/ROI).

285 **2.7 Mechanical testing**

286 Scaffolds were tested under unconfined compression using a TA.XTplus Texture Analyser
287 (Stable Microsystems) with a 500 g load cell. After careful removal of the fibrous tissue
288 around the scaffolds, the compression probe was brought in close contact with the sample
289 and a slight preload applied to ensure proper contact of the probe with the surface of the
290 sample. Samples were compressed to a strain of 15% at a loading rate of 0.01 mm per
291 second. The compressive modulus E was calculated as the slope of the linear range of the
292 stress-strain curve. It has to noted that, despite being careful and as accurate as possible
293 in removing the fibrous tissue, the difference in fibrous capsule thickness might have
294 affected the results of the mechanical testing and in particular for the softer, acellular
295 scaffolds.

296 **2.8 *Ultrasound and photo-acoustic imaging***

297 The Vevo LAZR (Visualsonics) system with a LZ550 transducer was used to perform high-
298 frequency ultrasound and photoacoustic imaging for the visualization and quantification
299 of scaffold volumes and oxygen saturation surrounding the implants. The images were
300 acquired 1 week post-surgery and right before sacrifice via excitation of the tissues with
301 high-frequency ultrasound waves for volume monitoring and with non-ionizing laser
302 pulses for blood flow analysis.

303 Oxy- and deoxy-hemoglobin absorb near infrared light differently, therefore
304 photoacoustic imaging can be used to generate a high-resolution parametric maps of the
305 oxygen saturation of blood in real-time. Total hemoglobin content was visualized by
306 exciting the tissue around the implant with laser pulses at 700nm while the oxygen
307 saturation was assessed using the Oxyhemo mode, a software algorithm that uses a dual
308 wavelength (750 and 850 nm) approach. The volumes of the scaffolds were calculated at
309 each time point by scanning the implant using the 3D mode with a motorized scan stage
310 at a step size of 0.2 mm. The scans were manually processed to identify the scaffold
311 contours and used to reconstruct the scaffold volumes.

312 The imaging is a non-invasive, painless procedure conducted under anesthesia that lasts
313 no longer than 30 minutes per animal assessments.

314 **2.9 *Serum inflammation marker analysis***

315
316 Mouse blood serum was prepared by clotting the whole blood for 2 hours at RT followed
317 by centrifugation at 3'000 rcf for 20 min at RT. The supernatant was then collected and
318 frozen at -80°C until further analysis. Values were normalized to baseline levels of serum
319 obtained 10 days before surgery.

- 320 • Multiplex assay. The serum concentrations of the cytokines IL-1 β , IL-4, IL-6, IL-10
321 and TNF- α as well as the C-reactive protein (CRP) were quantified using multiplex
322 immunoassay technology xMAP on a MAGPIX instrument (Luminex) according to
323 manufacturer's instructions. Mouse serum was diluted 1:2 with compatible
324 "Universal Assay Buffer" and measurements were performed with a custom-
325 designed multiplex assay kit (IL-1 β - EPX01A-26002-901; IL-4 - EPX01A-20613-
326 901; IL-6 - EPX01A-20603-901; IL-10 - EPX01A-20614-901; TNF- α - EPX01A-
327 20607-901, CRP - EPX01A-26045-901 ProcartaPlex assays; ThermoFisher).
328 Protein levels were measured in technical duplicates for each of the 36 animals.
329 The calibration was performed using a serial dilution of the standard mix provided
330 with the multiplex kit. Data were fitted using a four-parameter logistic regression
331 model. The quantification of the lower limit of detection (LOD) using this system
332 was 2.2, 0.2, 0.2, 0.1, 1 and 2.7 pg/ml for IL-10, IL-1 β , IL-4, IL-6 and TNF- α ,
333 respectively.
- 334 • Enzyme Linked Immunosorbent Assay (ELISA). Pentraxin 2 (PTX 2), also known
335 as Serum Amyloid P (SAP), and Serum Amyloid A (SAA) levels in mouse serum
336 were quantified using Quantikine[®] ELISA kits (MPTX20 and MSA00 respectively,
337 R&D Systems) according to manufacturer's instructions. For the SAA ELISA assay
338 mouse serum was diluted 1:200. For SAP analysis, serum was diluted 1:400 with
339 the exception of C57BL/6 serum that was diluted 1:100 due to different levels of
340 endogenous SAP.

341 **2.10 Statistical analysis**

342 All data are reported as mean \pm standard deviation. Statistical analysis was performed
343 with Matlab (Matlab 2017b, MathWorks). Comparison of results was carried out by 2-way
344 analysis of variance (ANOVA) using Tukey's multiple comparison post hoc test for
345 significance. The different mouse strains were compared between each other with
346 Bonferroni post-hoc tests and their statistical significance indicated in the graphs with
347 asterisks (* $p < 0.05$, ** $p < 0.01$, *** $p < 0.001$). The F values and the p values of the ANOVAs
348 are reported in the respective figure captions. Significant differences between the cellular
349 conditions were similarly assessed and are reported in the respective result sections.

350

351

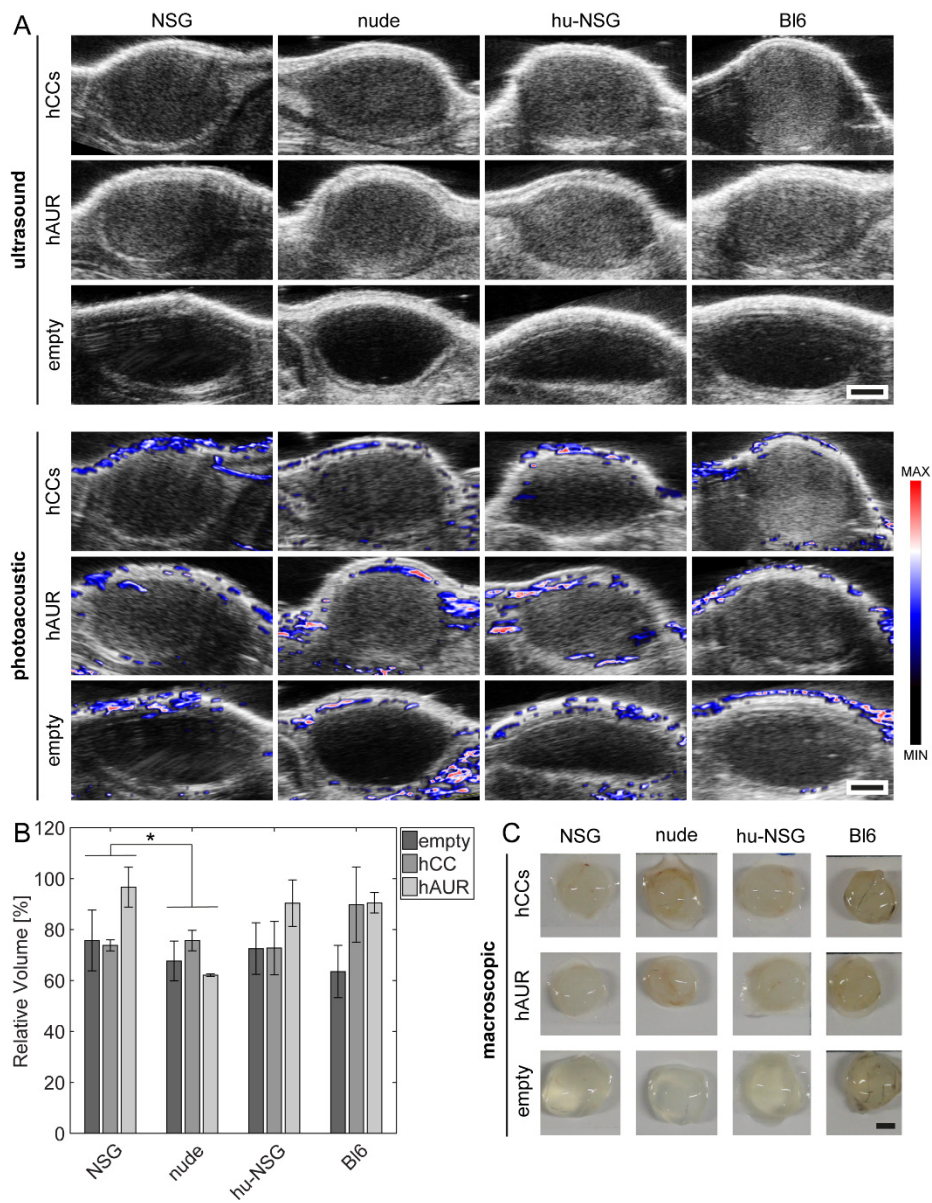
Results

352

2.1 Macroscopic appearance, volume retention and vascularization

353

of the scaffolds



354

355

356

357

358

Figure 2 A: Ultrasound and photoacoustic images of HA-TG constructs 4 weeks after implantation. Photoacoustic images are depicted as overlay of ultrasound and heat map of oxygen saturation. Scale bar: 1mm. B: Relative volume quantification (week 4/ week 1) of ultrasound images. Asterisk (* $p < 0.05$) indicates the statistical differences between mouse strains ($F(3,24) = 4.576, p = 0.011$). C: Macroscopic images of HA-TG hydrogels after explantation. Scale bar: 2mm

359 Ultrasound scans of cell-laden and acellular constructs (*Figure 2A*) revealed the
360 homogenous structure of the constructs with the cellular scaffolds being brighter than the
361 acellular ones, suggesting that those tissues are denser and with a lower fluid content,
362 likely due to their higher collagen content. The oxy-hemo photoacoustic images (*Figure*
363 *2B and Supplementary Figure 1*) of the constructs showed an absence of oxy-hemoglobin
364 inside the scaffolds. On the other hand, the tissue that surrounded them appeared to be
365 highly vascularized. Quantification of the ultrasound images acquired with the device's
366 3D mode showed that the scaffolds retained 60 to 95% of the initial volume. Acellular
367 scaffolds showed a reduction of volume compared to both hCC (* $p < 0.05$) and hAUR
368 (** $p < 0.001$) containing scaffolds. No statistically significant difference in volume
369 reduction was observed between the cellular conditions across mice while there was a
370 significant difference between NSG and nude mice (* $p < 0.05$).

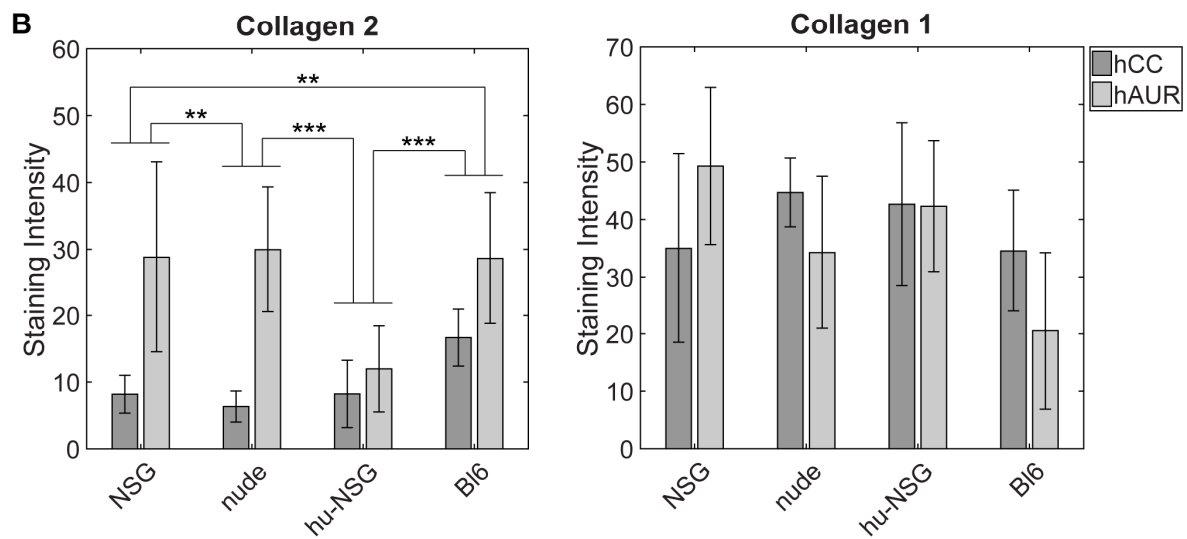
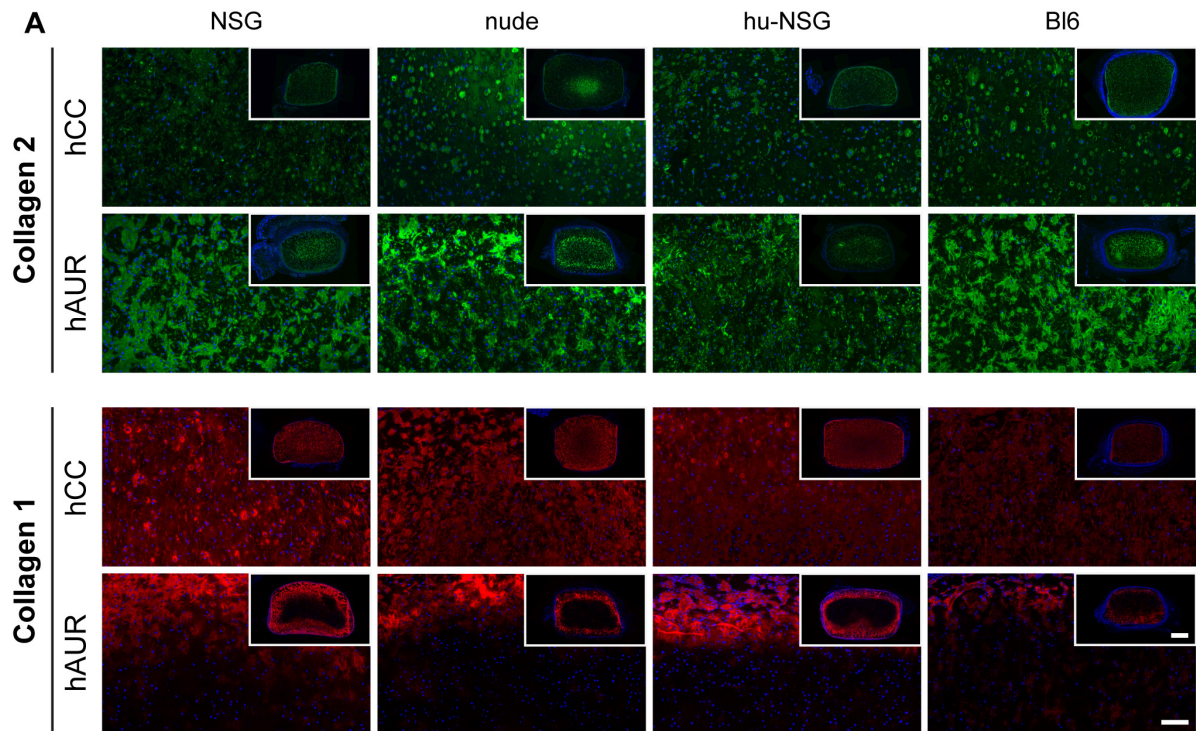
371 Shape retention and lack of vascularization could also be observed from the macroscopic
372 pictures (*Figure 2C*) of the constructs after explantation from mice. No adverse effects or
373 macroscopic signs of toxicity such as necrosis of nearby tissue, edema or hyperemia were
374 observed.

375 **2.2 Chondrogenesis of hCCs and hAURs in HA-TG hydrogels**

376 Both cellular conditions resulted in high amounts of extracellular matrix (ECM) produced
377 *in vitro* during pre-culture (*Supplementary Figure 3*). Yet, only hAUR were able to maintain
378 and/or produce collagen 2 consistently *in vivo* (*Figure 3*). In hAUR-seeded scaffolds
379 collagen 2 appeared homogeneously distributed throughout the constructs with a dense
380 ring in the outer border of the scaffolds implanted in nude animals. These results were

381 confirmed by semi-quantitative analysis of the staining intensities (hAUR vs. hCC,
382 *** $p < 0.001$).

383 Collagen 1 production was comparable in all mouse strains, while for hCC it was
384 homogeneously distributed through the cross section, for hAUR it was only present in the
385 outer border. The differences in collagen distributions could be due to a different cell
386 response to nutrients, growth factors and oxygen, although more studies will be required
387 to clarify it. The integrated density quantification showed no significant difference
388 between the mouse strains.

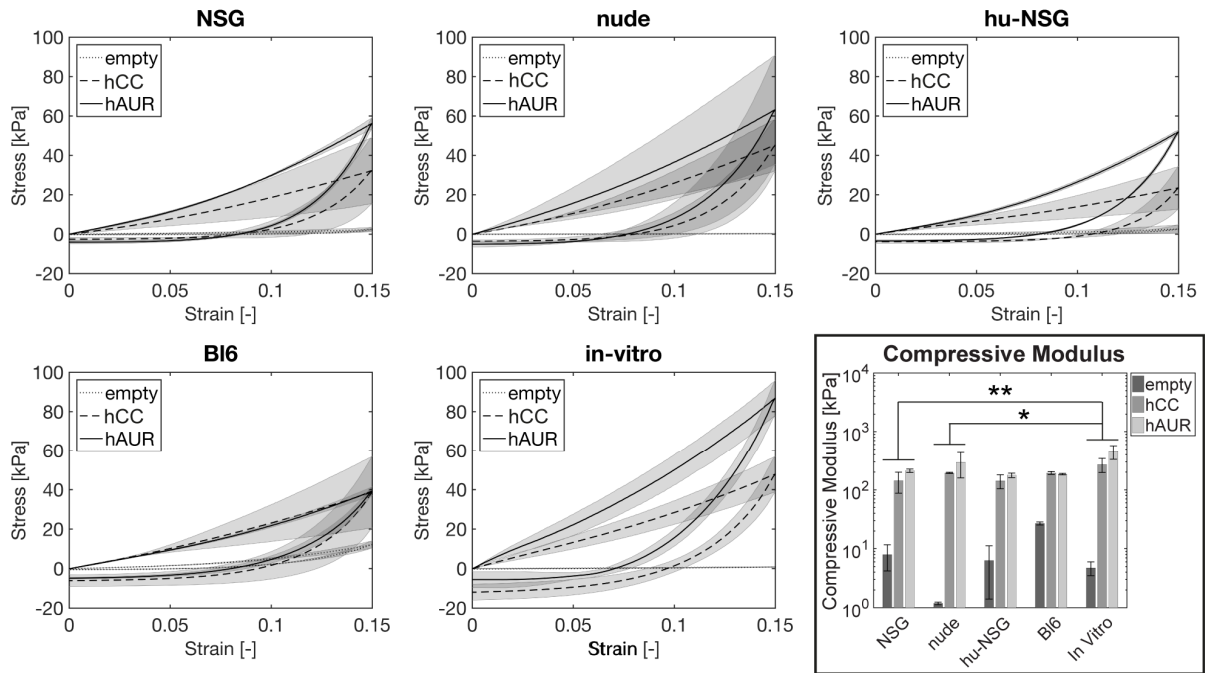


389

390 Figure 3 A: Collagen 2 and collagen 1 histological staining with DAPI counterstaining of cell-laden HA-TG hydrogels after
 391 4 weeks of in vitro pre-culture and 4 additional weeks in vivo. Scale bar close up: 100µm, scale bar insert: 500µm. B:
 392 Quantification of collagen stainings. The integrated density of the staining was used for semi-quantitative analysis of
 393 collagen 2 and 1. Asterisks (**p<0.01, ***p<0.001) indicate the statistical differences between mouse strains (F(3,60)=9.71,
 394 p<0.001 for collagen 2 and F(3,48)=6.10, p=0.001 for collagen 1).

395

2.3 Mechanical properties of HA-TG scaffolds



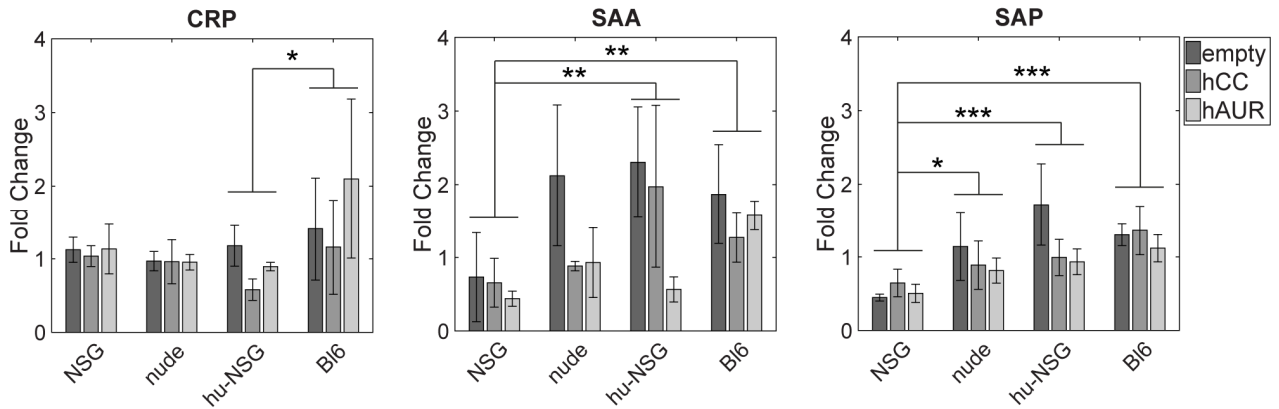
396

397 *Figure 4 Stress strain curves of compression tests from in vivo samples after explantation and in vitro samples after 49*
 398 *days. Compressive modulus of cellular and acellular samples corresponding to the depicted stress strain curves. Asterisks*
 399 *(* $p < 0.05$, ** $p < 0.01$) indicate the statistical differences between mouse strains and/or in vitro controls ($F(4,30)=8.38$,*
 400 *$p < 0.001$).*

401 A significant increase in compressive modulus of the constructs compared to the acellular
 402 gels was observed as a result of matrix produced by hCCs and hAUR (*Figure 4*). Acellular
 403 scaffolds *in vitro* maintained their mechanical strength over 7 weeks ($E = 4.7 \pm 1.2$ kPa)
 404 while acellular scaffolds *in vivo* displayed different behavior: samples implanted in NSG
 405 and hu-NSG mice maintained their strength ($E = 8.4 \pm 4.0$ kPa, $E = 7.0 \pm 5.4$ kPa,
 406 respectively), while samples implanted in nude mice decreased in strength compared to
 407 the time of implantation ($E = 1.2 \pm 0.1$ kPa) and samples implanted in C57BL/6 increased
 408 in strength ($E = 30.4 \pm 1.6$ kPa). Both cell types led to a significantly higher modulus
 409 compared to acellular scaffolds (** $p < 0.001$) and hAUR performed significantly better
 410 than hCCs (** $p < 0.001$). All mouse strains led to comparable compressive moduli, with

411 only NSG and nude mice resulting in significantly lower moduli than in vitro controls
412 (**p<0.01 and *p<0.05).

413 2.4 Inflammation markers



414

415 *Figure 5 Acute phase inflammation markers CRP, SAA and SAP detected in mouse serum 4 weeks post-implantation and*
416 *normalized to baseline values acquired 10 days before surgery. Asterisks (*p<0.05, **p<0.01, ***p<0.001) indicate the*
417 *statistical differences between mouse strains (F(3,24)=3.96, p=0.020 for CRP, F(3,24)=5.73, p=0.004 for SAA, F(3,24)=12.42,*
418 *p<0.001 for SAP).*

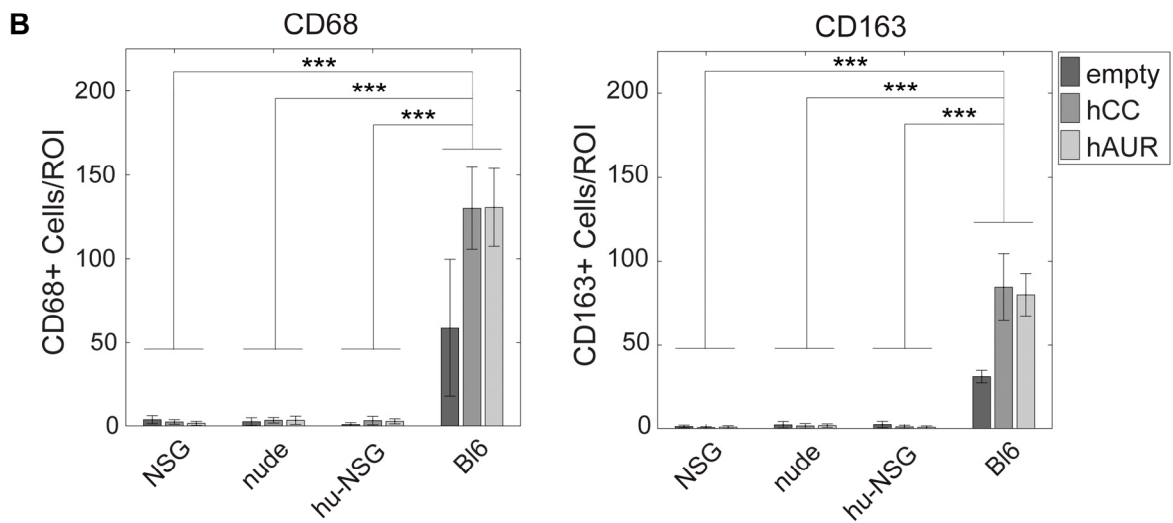
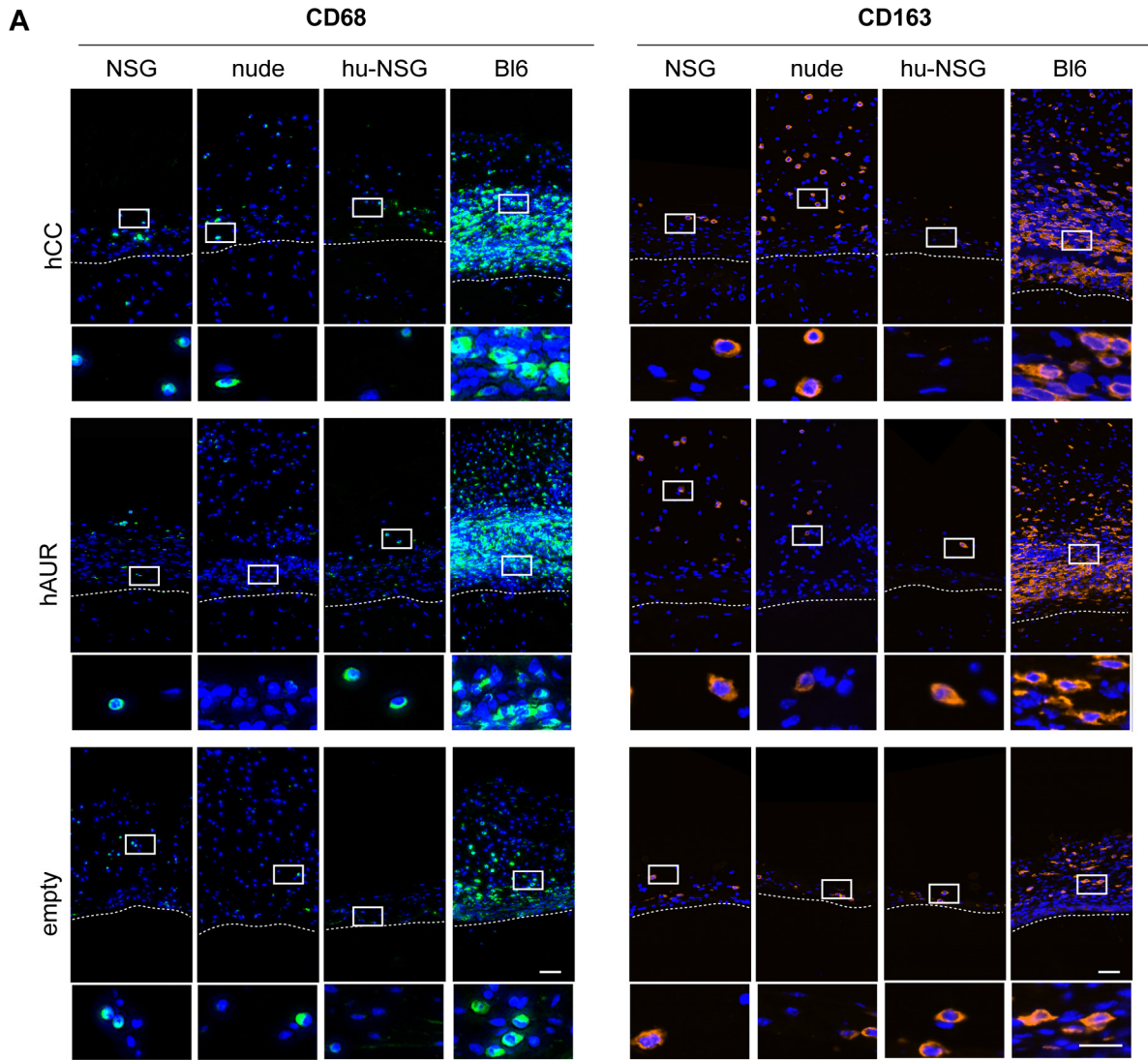
419 CRP, SAA and SAP are acute phase proteins (APP), primarily synthesized by hepatocytes as
420 part of the acute phase response [29]. Although not specific, APP upregulation is triggered by
421 different stimuli including trauma, infection, stress and inflammation with the goal of
422 reestablishing homeostasis [30, 31]. In mice SAA and SAP are considered major acute
423 phase proteins, meaning that they can be increased 10- to 100-fold. CRP, on the other hand, is
424 a moderate acute phase protein and can be upregulated 2- to 10-fold following a stimuli [29,
425 32].

426 CRP levels in serum (*Figure 5*) at 4 weeks after surgery showed no increase to baseline
427 levels (*Supplementary Table 3*) in NSG, nude and humanized NSG-SGM3 mice. 2.0 ± 1.0
428 and 1.4 ± 0.7 fold increase were observed in C56BL/6 mice for hAUR and acellular
429 scaffolds respectively. No significant differences were observed between the cellular and

430 acellular conditions across strains and, although hCC seeded scaffolds routinely showed
431 lower CRP values, they were not significantly different.

432 SAA levels in serum (*Figure 5*) were significantly higher (** $p < 0.01$) in humanized NSG-
433 SGM3 and C56BL/6 mice (2.2 ± 1.1 for hCC, 0.56 ± 0.2 for hAUR, 2.0 ± 0.8 for acellular and
434 1.3 ± 0.3 for hCC, 1.6 ± 0.2 for hAUR, 1.8 ± 0.7 for acellular respectively) than NSG ($0.7 \pm$
435 0.5 for hCC, 0.4 ± 0.1 for hAUR, 0.7 ± 0.6 for acellular). Both cell-loaded scaffolds led to an
436 overall downregulation of SAA levels compared to acellular scaffolds (with hAUR showing
437 a significant difference to acellular, ** $p < 0.01$). SAP levels in serum (*Figure 5*) followed a
438 similar trend, with the lowest values found in NSG mice (0.9 ± 0.3 for hCC, 0.7 ± 0.2 for
439 hAUR, 1.3 ± 0.3 for acellular) and the highest in C56BL/6 mice (1.4 ± 0.3 for hCC, 1.1 ± 0.2
440 for hAUR, 1.3 ± 0.1 for acellular). Similarly, hAUR and hCC led to an overall
441 downregulation of SAP levels compared to acellular scaffolds ($*p < 0.05$ for hAUR vs
442 acellular) showing that cellular associations have a positive effect on the biomaterial
443 implantation.

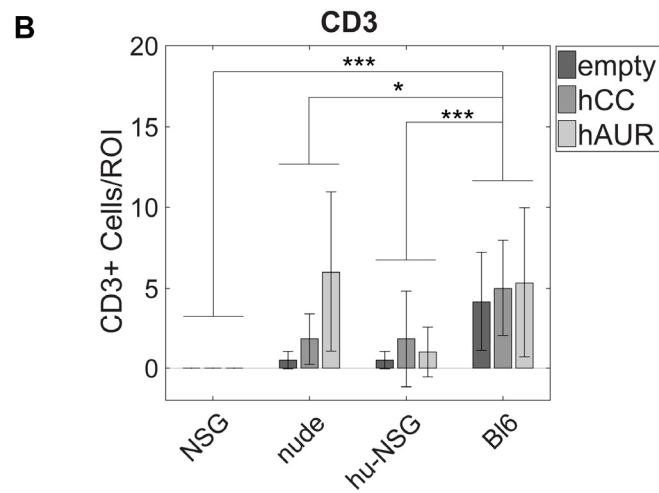
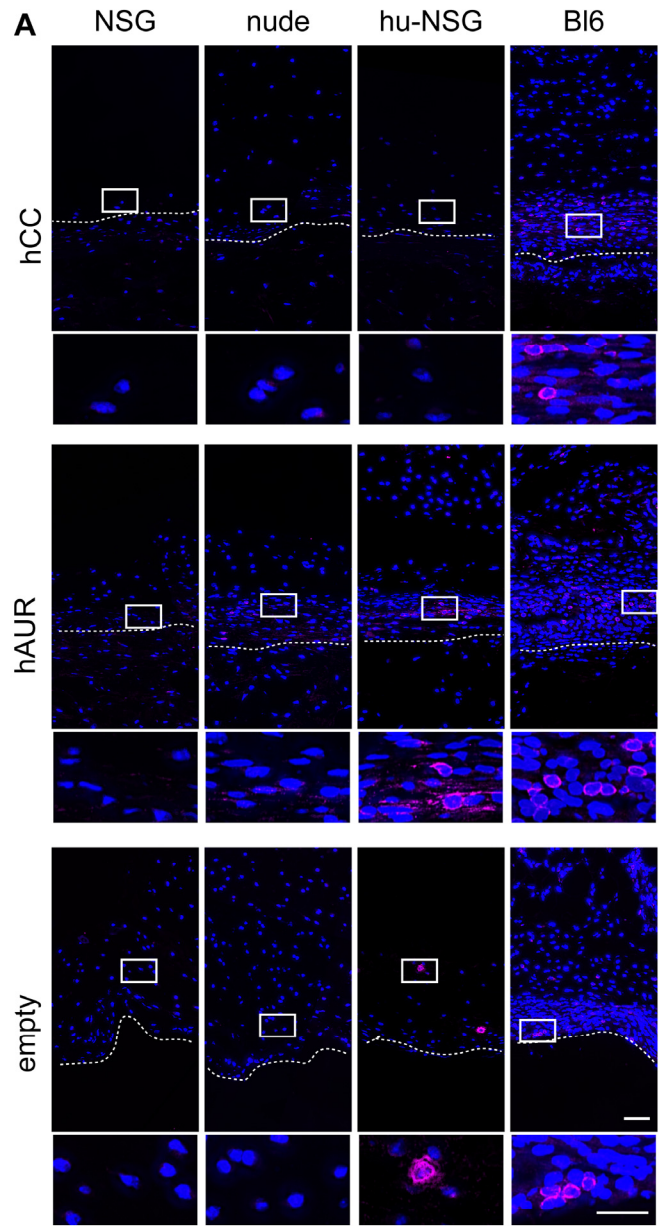
2.5 Macrophage presence and infiltration



446 *Figure 6 A: CD68 and CD163 histological staining with DAPI counterstaining. Images being cross-sections of the scaffolds*
447 *and fibrous capsule with the scaffolds in the bottom part of the image, below the dotted white lines. Scale bar: 50 μm. .*
448 *Higher magnification is provided at the bottom of each image. Scale bar: 100 μm. B: Quantification of CD68 and CD163*
449 *positive cells per region of interest (ROI). Asterisk (**p<0.001) indicates the statistical differences between mouse strains*
450 *(F(3,60)=203.45, p<0.001 for CD68, F(3,60)=381.03, p<0.00 for CD163).*

451 CD68 (Cluster of Differentiation 68) and CD163 (Cluster of Differentiation 163) are
452 transmembrane glycoproteins expressed by cells in the monocyte and macrophage
453 lineages [33, 34]. CD68 and CD163 are used to identify macrophages in tissue sections
454 with CD163 positive cells usually considered as M2 (anti-inflammatory) macrophages
455 [35]. A significantly higher (**p<0.001) number of both CD68+ and CD163+ cells was
456 observed in the fibrous capsule around the scaffolds implanted in C57BL/6 mice
457 compared to the other mouse strains (*Figure 6*). For both markers, a significantly lower
458 (**p<0.001) number of positive cells was found around the acellular scaffolds compared
459 to both hAUR and hCC scaffolds. No macrophage infiltration into samples was observed
460 in any of the conditions but a thicker fibrous capsule was observed in C57BL/6 mice
461 around the scaffolds.

2.6 *Lymphocyte presence*



464 *Figure 7 CD3 histological staining with DAPI counterstaining. Images being cross-sections of the scaffolds and fibrous*
465 *capsule with the scaffolds in the bottom part of the image, below the dotted white lines. Scale bar: 50 μ m. Higher*
466 *magnification is provided at the bottom of each image. Scale bar: 100 μ m. B: Quantification of CD3 positive cells per region*
467 *of interest (ROI). Asterisk (* $p < 0.05$, *** $p < 0.001$) indicates the statistical differences between mouse strains ($F(3,60) = 12.18$,*
468 *$p < 0.001$).*

469 The CD3 (Cluster of differentiation 3) is part of the T cell receptor complex of mature T
470 lymphocytes and is used in immunology to identify both the cytotoxic T cells (CD8+) and
471 the T helper cells (CD4+). As expected, no CD3+ cells could be found in the fibrous tissue
472 surrounding the scaffolds implanted in NSG mice, however a limited amount of CD3+ cells
473 could be found in the humanized mouse samples (*Figure 7*). Given that the humanized mice
474 are developed from NSG animals and have relatively high human engraftment, the lymphocytes
475 that were found in the histological sections from samples implanted in humanized animals can
476 be considered from human origin. Despite their lack of thymus, some lymphocytes could be
477 observed in the nude mouse samples. Extrathymic maturation of T cells has been documented
478 in nude mice and an increasing number of CD3+ cells correlates with the mouse age [36]. Not
479 surprisingly, the highest number of CD3+ cells could be identified in C57BL/6 mice (* $p < 0.05$
480 to nude, * $p < 0.001$ to NSG and to hu-NSG).

481

482 **3. Discussion**

483 Despite the critical role that mouse studies play in providing cost and time effective proof-
484 of-concept data, there is no unanimity on the optimal mouse strain for cartilage
485 regeneration studies [37]. This could be attributed to several reasons. Firstly, there are
486 no regulatory guidelines for conducting cartilage engineering studies in small animal
487 models. Secondly, the use of human cells often limits the choice to immunodeficient
488 animals [38]. Lastly, despite cartilage being considered immune-privileged [39, 40], there
489 is a lack of understanding of how the host immune system affects chondrogenesis *in vivo*
490 [41]. The recent advances in the development of humanized mice has further increased
491 the range of possible mouse strains to choose from. The advancement of humanized mice
492 raised the question of whether those could represent a suitable animal model to bridge
493 the gap between mouse and human studies at least for pre-screening purposes. In this
494 study, we evaluated the chondrogenic potential of xenogenic, tissue-engineered grafts by
495 implanting it subcutaneously in mice that present varying immune systems.

496 The HA-TG hydrogel system has already proven to be biocompatible, mitogenic and
497 adhesive to cartilage tissue. In addition, it induces cartilaginous matrix deposition by
498 encapsulated human chondroprogenitor cells *in vitro* [22]. In this study, we were able to
499 show that HA-TG supports human auricular chondrocyte survival and extracellular
500 matrix deposition *in vitro* and *in vivo*. Both cellular and acellular HA-TG hydrogels did not
501 degrade and resisted vascular and cellular infiltration for up to 4 weeks *in vivo*.
502 Importantly, as reflected by the increase in mechanical strength and collagen 2 content,
503 HA-TG hydrogels supported ECM production by both adult (hAUR) and
504 chondroprogenitor (hCC) chondrocytes independently of the mouse strains.

505 Furthermore, in hAUR-seeded scaffold, HA-TG induced the synthesis of a collagen 2-rich
506 ECM while keeping low expression levels of collagen 1.

507 Different *in vitro* results were seen with hCC seeded scaffolds as high levels of collagen 2
508 were not maintained *in vivo*. The differences of hCC to preserve the matrix that was
509 produced during *in vitro* preculture could be due to several factors. The collagen 2
510 produced *in vitro* might not be sufficiently mature and crosslinked [42] and therefore
511 diffuse out of the hydrogel once *in vivo*, however mechanical testing would suggest
512 otherwise. hCC have been shown to undergo a certain degree of spontaneous
513 differentiation (i.e. without stimulation by growth factors) towards the chondrogenic
514 lineage [24], however their chondrogenic potential can be impaired in the absence of TGF-
515 β growth factors (data not shown). On the other hand, hAURs were fully differentiated
516 before implantation and therefore had a more stable phenotype and did not required
517 exogenous supplementation of TGF- β . No obvious inflammatory infiltrates or foreign-body
518 reactions were observed at histological examination but host cytokines and the
519 surrounding subcutaneous environment could contribute to cell death and/or phenotype
520 instability [43]. Although it remains unclear whether the same cells would make durable
521 cartilage tissue when implanted into a cartilage-inducing/maintaining environment, such
522 as an articular cartilage defect, ex-vivo studies showed promising results [22]. Moreover,
523 there are differences for the two investigated cell types as they have different origins
524 during embryonic development [44]. While articular chondrocytes develop from the
525 mesoderm, auricular chondrocytes originate from the neural crest. Cells from the neural
526 crest have the capacity to generate various cell and tissue types even across germ layers
527 [45] and are known for their multipotency and ability to undergo chondrogenic
528 differentiation in heterotopic transplantation sites [46]. Therefore, the two cell types have

529 a different stability depending on the environment and mechanical/biochemical
530 stimulation that they will receive upon transplantation.

531 C57BL/6 mice have complete innate and adaptive immune systems. Not surprisingly,
532 systemic inflammation markers (CRP, SAA and SAP: *Figure 5*; IL6, IL10 and TNF- α :
533 *Supplementary Figure 6*) were consistently upregulated in C57BL/6 animals and a higher
534 number of macrophages and lymphocytes (*Figure 6* and *Figure 7* respectively), together
535 with a larger fibrous capsule, was found around the implants in comparison to
536 immunodeficient and humanized mice. In addition to their phagocytic properties,
537 macrophages actively regulate tissue repair by secreting various cytokines, growth
538 factors, ECM components and proteases [47]. HA-TG is synthesized from high molecular
539 weight hyaluronic acid (HA) which has been documented as antiangiogenic, antioxidant
540 as well as anti-inflammatory [48]. A CD163 macrophage-mediated reaction to high
541 molecular weight HA might have reduced inflammation and promoted chondrogenesis in
542 immunocompetent animals, as indicated by the higher collagen 2 production observed in
543 this strain [49]. Another factor that could have played a role is the thicker fibrous capsule
544 which might have produced a more hypoxic environment compared to the capsules
545 observed in the immunodeficient and humanized mice and therefore led to a stronger
546 chondrogenesis [50]. The stronger innate immune response observed in the C57BL/6
547 mice, compared to humanized mice, could also be due to the fact that the former is a
548 xenogeneic reaction, while the latter is allogeneic. Indeed, xenogeneic transplantation of
549 human chondrocytes have been reported to be rejected by minipigs [51] and rabbits [39] and
550 the transplanted cells failed to undergo chondrogenesis in vivo despite allogenic transplantation
551 could be successfully performed [39].

552 Previous studies reported mixed outcomes of ectopic cartilage reconstruction and bone
553 regeneration in immunocompetent small animals [38, 52-55]. Failures in chondrogenesis
554 and osteogenesis were attributed to immune reaction of the host to the allogenic
555 materials and cells, but also to vascular invasion that cause construct degradation and
556 host tissue ingrowth [56]. The absence of T-cells in nude animals was suspected to be the
557 reason for reduced cytotoxic mechanisms associated with macrophages and soluble
558 factors, including complements and antibodies [57]. HA-TG resistance to cellular and
559 vascular infiltration could explain why chondrogenesis of hAUR in immunocompetent
560 C57BL/6 animals was comparable to that of in immunodeficient mice. In addition, HA-TG
561 is a naturally derived material which is degraded by MMPs and hydrolytic enzymes in low
562 molecular weight hyaluronan molecules [58]. The non-toxicity of its degradation products
563 exclude another common reason of chondrogenic failure [59].

564 This study provides an insight on the role of the murine immune system in subcutaneous
565 implantation of cartilage engineering scaffolds. Overall, we observed a similar trend in the
566 development of the scaffolds in all four mouse strains in terms of mechanical
567 strengthening of the grafts and ECM expression. Our results suggest that despite being
568 subjected to a functional immune system, chondrogenesis still occurs in samples
569 implanted in C57BL/6 and that, despite being subjected to a humanized immune system
570 in NSG-SGM3, chondrogenesis still occurs albeit not as strongly as in the other mouse
571 strains. Nevertheless there are some limitations to our study. Even though our results
572 were reproducible among the biological replicates, studies with larger sample size would
573 be needed for validation. The inflammation markers were analyzed by multiplex assay on
574 serum whereby several cytokines were below the lower limit of detection and therefore
575 a subcutaneous tissue cage model [60] utilizing the analysis of exudate could be better

576 suited for this purpose. Finally, more research is required to develop reliable humanized
577 mice (i.e. with a stronger humanized innate immune response and in particular with an
578 increased number of macrophages and natural killer cells) and to systematically evaluate
579 how mouse studies translate into large animal models and humans.

580 **4. Conclusions**

581 To our knowledge, this is the first study that compared the chondrogenic potential of a
582 tissue-engineered construct for cartilage regeneration in several mouse strains. In
583 addition, this is the earliest attempt to use a humanized mouse model in the cartilage
584 engineering field. Collectively the results of this study suggest that chondrogenesis of a
585 tissue-engineered cartilage graft is feasible in immunocompetent small animals. We
586 suggest that immunocompetent and immunodeficient animals could lead to analogous
587 results in terms of chondrogenesis, as long as the implanted cells are shielded from the
588 host by a biomaterial. Preclinical investigation in immunocompetent animals is an
589 essential step in the clinical translation of orthopedic scaffolds [59, 61] and
590 immunodeficient rodent models are still the model of choice for early testing procedures
591 and screening. Subcutaneous implantation in small animals with a complete and human
592 immune system could help understanding how tissue-engineered constructs perform
593 with an active immune system.

594 **5. Acknowledgments**

595 This work was supported by the ETH Zurich Foundation (Grant No. ETH-50 13-1), by a
596 Competence Center for Applied Biotechnology and Molecular Medicine (CABMM) startup
597 grant and partly by the Sandoz Family Foundation. We acknowledge the help of the
598 Scientific Center for Optical and Electron Microscopy (ScopeM) of ETH Zurich. The

599 authors acknowledge Dr. Matti Kesti for the initial discussions about the project, Nicolas
600 Broguiere for the help with HA-TG synthesis and characterization and David Fercher for
601 his help with cell culture. The authors are grateful to Prof. Emma Wetter Slack for the
602 fruitful discussions.

603 **6. Author contributions**

604 This study was designed by E.C., P.F., R.G. and M.Z.W.; acquisition of all data was conducted
605 by E.C., P.F. and F.A.F.; animal experiments were performed by E.C., P.F. and M.Z.W.; data
606 analysis was performed by E.C., P.F. and F.A.F.. All authors were involved in interpreting
607 the data, drafting the article, revising the manuscript for important intellectual content,
608 and approved the final version to be submitted.

609 **7. Disclosure Statement**

610 Marcy Zenobi-Wong serves as a consultant for Auregen S.A. . Ralph Gareus is an employee
611 of The Jackson Laboratory.

612

8. References

- 614 1. Piedrahita, J.A. and J.K. Williams, *Animal Models in Tissue Engineering. Part I. Tissue*
615 *Eng Part C Methods*, 2017. **23**(11): p. 641-642.
- 616 2. Cook, J.L., et al., *Animal models of cartilage repair*. *Bone Joint Res*, 2014. **3**(4): p. 89-
617 94.
- 618 3. Makris, E.A., et al., *Repair and tissue engineering techniques for articular cartilage*.
619 *Nature Reviews Rheumatology*, 2015. **11**(1): p. 21-34.
- 620 4. Ha, C.W., et al., *Initial phase I safety of retrovirally transduced human chondrocytes*
621 *expressing transforming growth factor-beta-1 in degenerative arthritis patients*.
622 *Cytotherapy*, 2012. **14**(2): p. 247-256.
- 623 5. Lee, M.C., et al., *A placebo-controlled randomised trial to assess the effect of TGF-beta*
624 *1-expressing chondrocytes in patients with arthritis of the knee (vol 97, pg 924,*
625 *2015)*. *Bone & Joint Journal*, 2015. **97b**(12): p. 1732-1732.
- 626 6. Cherian, J.J., et al., *Preliminary results of a phase II randomized study to determine*
627 *the efficacy and safety of genetically engineered allogeneic human chondrocytes*
628 *expressing TGF-beta 1 in patients with grade 3 chronic degenerative joint disease of*
629 *the knee*. *Osteoarthritis and Cartilage*, 2015. **23**(12): p. 2109-2118.
- 630 7. Farr, J. and J.Q. Yao, *Chondral Defect Repair with Particulated Juvenile Cartilage*
631 *Allograft*. *Cartilage*, 2011. **2**(4): p. 346-53.
- 632 8. Buckwalter, J.A., et al., *Clinical outcomes of patellar chondral lesions treated with*
633 *juvenile particulated cartilage allografts*. *Iowa Orthop J*, 2014. **34**: p. 44-9.
- 634 9. Bugbee, W.D., et al., *Osteochondral allograft transplantation in cartilage repair:*
635 *Graft storage paradigm, translational models, and clinical applications*. *J Orthop*
636 *Res*, 2016. **34**(1): p. 31-8.
- 637 10. Whitelaw, C.B., et al., *Engineering large animal models of human disease*. *J Pathol*,
638 2016. **238**(2): p. 247-56.
- 639 11. Chu, C.R., M. Szczodry, and S. Bruno, *Animal models for cartilage regeneration and*
640 *repair*. *Tissue Eng Part B Rev*, 2010. **16**(1): p. 105-15.
- 641 12. Reinholz, G.G., et al., *Animal models for cartilage reconstruction*. *Biomaterials*, 2004.
642 **25**(9): p. 1511-21.
- 643 13. Segre, J.A., et al., *Positional cloning of the nude locus: genetic, physical, and*
644 *transcription maps of the region and mutations in the mouse and rat*. *Genomics*,
645 1995. **28**(3): p. 549-59.
- 646 14. Shultz, L.D., et al., *Human lymphoid and myeloid cell development in NOD/LtSz-scid*
647 *IL2R gamma null mice engrafted with mobilized human hemopoietic stem cells*. *J*
648 *Immunol*, 2005. **174**(10): p. 6477-89.
- 649 15. Shultz, L.D., F. Ishikawa, and D.L. Greiner, *Humanized mice in translational*
650 *biomedical research*. *Nat Rev Immunol*, 2007. **7**(2): p. 118-30.
- 651 16. Kitchen, S.G., et al., *In Vivo Suppression of HIV by Antigen Specific T Cells Derived*
652 *from Engineered Hematopoietic Stem Cells*. *Plos Pathogens*, 2012. **8**(4).

- 653 17. McDermott, S.P., et al., *Comparison of human cord blood engraftment between*
654 *immunocompromised mouse strains*. *Blood*, 2010. **116**(2): p. 193-200.
- 655 18. Billerbeck, E., et al., *Development of human CD4+FoxP3+ regulatory T cells in human*
656 *stem cell factor-, granulocyte-macrophage colony-stimulating factor-, and*
657 *interleukin-3-expressing NOD-SCID IL2Rgamma(null) humanized mice*. *Blood*, 2011.
658 **117**(11): p. 3076-86.
- 659 19. Walsh, N.C., et al., *Humanized Mouse Models of Clinical Disease*. *Annual Review of*
660 *Pathology: Mechanisms of Disease*, Vol 12, 2017. **12**: p. 187-215.
- 661 20. Ito, R., et al., *Current advances in humanized mouse models*. *Cellular & Molecular*
662 *Immunology*, 2012. **9**(3): p. 208-214.
- 663 21. Carrillo, M.A., A.J. Zhen, and S.G. Kitchen, *The Use of the Humanized Mouse Model in*
664 *Gene Therapy and Immunotherapy for HIV and Cancer*. *Frontiers in Immunology*,
665 2018. **9**.
- 666 22. Broguiere, N., et al., *Factor XIII Cross-Linked Hyaluronan Hydrogels for Cartilage*
667 *Tissue Engineering*. *ACS Biomaterials Science & Engineering*, 2016. **2**(12): p. 2176-
668 2184.
- 669 23. Broguiere, N., L. Isenmann, and M. Zenobi-Wong, *Novel enzymatically cross-linked*
670 *hyaluronan hydrogels support the formation of 3D neuronal networks*. *Biomaterials*,
671 2016. **99**: p. 47-55.
- 672 24. Darwiche, S., et al., *Epiphyseal Chondroprogenitors Provide a Stable Cell Source for*
673 *Cartilage Cell Therapy*. *Cell Med*, 2012. **4**(1): p. 23-32.
- 674 25. Studer, D., et al., *Human chondroprogenitors in alginate-collagen hybrid scaffolds*
675 *produce stable cartilage in vivo*. *J Tissue Eng Regen Med*, 2017. **11**(11): p. 3014-
676 3026.
- 677 26. Adkisson, H.D.t., et al., *The potential of human allogeneic juvenile chondrocytes for*
678 *restoration of articular cartilage*. *Am J Sports Med*, 2010. **38**(7): p. 1324-33.
- 679 27. Bell, S.P., et al., *Reduced Subendocardial Perfusion Correlates with Impaired Energy*
680 *Supply-Demand Relations in Patients with Non-Ischemic Dilated Cardiomyopathy*.
681 *Circulation*, 2010. **122**(21).
- 682 28. Snider, T.N. and Y. Mishina, *Cranial neural crest cell contribution to craniofacial*
683 *formation, pathology, and future directions in tissue engineering*. *Birth Defects Res*
684 *C Embryo Today*, 2014. **102**(3): p. 324-32.
- 685 29. Cray, C., J. Zaias, and N.H. Altman, *Acute phase response in animals: a review*. *Comp*
686 *Med*, 2009. **59**(6): p. 517-26.
- 687 30. Murata, H., N. Shimada, and M. Yoshioka, *Current research on acute phase proteins*
688 *in veterinary diagnosis: an overview*. *Vet J*, 2004. **168**(1): p. 28-40.
- 689 31. Petersen, H.H., J.P. Nielsen, and P.M. Heegaard, *Application of acute phase protein*
690 *measurements in veterinary clinical chemistry*. *Vet Res*, 2004. **35**(2): p. 163-87.
- 691 32. Ceron, J.J., P.D. Eckersall, and S. Martinez-Subiela, *Acute phase proteins in dogs and*
692 *cats: current knowledge and future perspectives*. *Veterinary Clinical Pathology*,
693 2005. **34**(2): p. 85-99.

- 694 33. Holness, C.L. and D.L. Simmons, *Molecular cloning of CD68, a human macrophage*
695 *marker related to lysosomal glycoproteins*. Blood, 1993. **81**(6): p. 1607-13.
- 696 34. Lau, S.K., P.G. Chu, and L.M. Weiss, *CD163: a specific marker of macrophages in*
697 *paraffin-embedded tissue samples*. Am J Clin Pathol, 2004. **122**(5): p. 794-801.
- 698 35. Barros, M.H., et al., *Macrophage polarisation: an immunohistochemical approach for*
699 *identifying M1 and M2 macrophages*. PLoS One, 2013. **8**(11): p. e80908.
- 700 36. Kennedy, J.D., C.W. Pierce, and J.P. Lake, *Extrathymic T-Cell Maturation - Phenotypic*
701 *Analysis of T-Cell Subsets in Nude-Mice as a Function of Age*. Journal of Immunology,
702 1992. **148**(6): p. 1620-1629.
- 703 37. Moran, C.J., et al., *The benefits and limitations of animal models for translational*
704 *research in cartilage repair*. J Exp Orthop, 2016. **3**(1): p. 1.
- 705 38. Pomerantseva, I., et al., *Ear-Shaped Stable Auricular Cartilage Engineered from*
706 *Extensively Expanded Chondrocytes in an Immunocompetent Experimental Animal*
707 *Model*. Tissue Eng Part A, 2016. **22**(3-4): p. 197-207.
- 708 39. Arzi, B., et al., *Cartilage immunoprivilege depends on donor source and lesion*
709 *location*. Acta Biomater, 2015. **23**: p. 72-81.
- 710 40. Revell, C.M. and K.A. Athanasiou, *Success rates and immunologic responses of*
711 *autogenic, allogenic, and xenogenic treatments to repair articular cartilage defects*.
712 Tissue Eng Part B Rev, 2009. **15**(1): p. 1-15.
- 713 41. Bolano, L. and J.A. Kopta, *The Immunology of Bone and Cartilage Transplantation*.
714 Orthopedics, 1991. **14**(9): p. 987-996.
- 715 42. Athens, A.A., E.A. Makris, and J.C. Hu, *Induced collagen cross-links enhance cartilage*
716 *integration*. PLoS One, 2013. **8**(4): p. e60719.
- 717 43. De Bari, C., F. Dell'Accio, and F.P. Luyten, *Failure of in vitro-differentiated*
718 *mesenchymal stem cells from the synovial membrane to form ectopic stable cartilage*
719 *in vivo*. Arthritis Rheum, 2004. **50**(1): p. 142-50.
- 720 44. Pelttari, K., et al., *Nasal chondrocytes as a neural crest-derived cell source for*
721 *regenerative medicine*. Current Opinion in Biotechnology, 2017. **47**: p. 1-6.
- 722 45. Baggiolini, A., et al., *Premigratory and migratory neural crest cells are multipotent*
723 *in vivo*. Cell Stem Cell, 2015. **16**(3): p. 314-22.
- 724 46. Le Douarin, N.M., et al., *Neural crest cell plasticity and its limits*. Development, 2004.
725 **131**(19): p. 4637-50.
- 726 47. Wynn, T.A. and K.M. Vannella, *Macrophages in Tissue Repair, Regeneration, and*
727 *Fibrosis*. Immunity, 2016. **44**(3): p. 450-462.
- 728 48. Masuko, K., et al., *Anti-inflammatory effects of hyaluronan in arthritis therapy: Not*
729 *just for viscosity*. International Journal of General Medicine, 2009. **2**: p. 77-81.
- 730 49. Julier, Z., et al., *Promoting tissue regeneration by modulating the immune system*.
731 Acta Biomaterialia, 2017. **53**: p. 13-28.
- 732 50. Meretoja, V.V., et al., *The effect of hypoxia on the chondrogenic differentiation of co-*
733 *cultured articular chondrocytes and mesenchymal stem cells in scaffolds*.
734 Biomaterials, 2013. **34**(17): p. 4266-73.

- 735 51. Niemietz, T., et al., *Xenogeneic transplantation of articular chondrocytes into full-*
736 *thickness articular cartilage defects in minipigs: fate of cells and the role of*
737 *macrophages*. Cell Tissue Res, 2014. **358**(3): p. 749-61.
- 738 52. Britt, J.C. and S.S. Park, *Autogenous tissue-engineered cartilage - Evaluation as an*
739 *implant material*. Archives of Otolaryngology-Head & Neck Surgery, 1998. **124**(6):
740 p. 671-677.
- 741 53. Shieh, S.J., S. Terada, and J.P. Vacanti, *Tissue engineering auricular reconstruction:*
742 *in vitro and in vivo studies*. Biomaterials, 2004. **25**(9): p. 1545-1557.
- 743 54. Cao, Y.L., et al., *Comparative study of the use of poly(glycolic acid), calcium alginate*
744 *and pluronics in the engineering of autologous porcine cartilage*. Journal of
745 Biomaterials Science-Polymer Edition, 1998. **9**(5): p. 475-487.
- 746 55. Zhang, Y., et al., *Comparing immunocompetent and immunodeficient mice as animal*
747 *models for bone tissue engineering*. Oral Diseases, 2015. **21**(5): p. 583-592.
- 748 56. Zheng, L., et al., *In Vivo Cartilage Engineering with Collagen Hydrogel and*
749 *Allogeneous Chondrocytes After Diffusion Chamber Implantation in*
750 *Immunocompetent Host*. Tissue Engineering Part A, 2009. **15**(8): p. 2145-2153.
- 751 57. Kanazawa, S., et al., *Tissue responses against tissue-engineered cartilage consisting*
752 *of chondrocytes encapsulated within non-absorbable hydrogel*. Journal of Tissue
753 Engineering and Regenerative Medicine, 2013. **7**(1): p. 1-9.
- 754 58. Necas, J., et al., *Hyaluronic acid (hyaluronan): a review*. Veterinarni Medicina, 2008.
755 **53**(8): p. 397-411.
- 756 59. Liu, W. and Y.L. Cao, *Application of scaffold materials in tissue reconstruction in*
757 *immunocompetent mammals: Our experience and future requirements*.
758 Biomaterials, 2007. **28**(34): p. 5078-5086.
- 759 60. Chisholm, G.D., *The tissue cage model in the distribution of antibacterial agents*.
760 Scand J Infect Dis Suppl, 1978(14): p. 118-24.
- 761 61. Liu, Y., G.D. Zhou, and Y.L. Cao, *Recent Progress in Cartilage Tissue Engineering-Our*
762 *Experience and Future Directions*. Engineering, 2017. **3**(1): p. 28-35.
- 763
- 764

765

Supplementary information

766
767

Table 1 Flow cytometry quantification of human cell engraftment in NSG-SGM3. Data were obtained 12 weeks after birth (8 weeks after engraftment).

hCD45+ [total %]	hCD19+ (B cells) [% of hCD45]	hCD3+ (T cells) [% of hCD45]	hCD33+ (myeloid) [% of hCD45]	hCD45- [total %]
28 ±2.4	60.5±16.4	19.9±20.3	12.1±4.3	67.3±14.4

768

769
770

Table 2 HLA typing of the human donor used to engraft the humanized mice in the study, of the human chondroprogenitor cells (hCCs) and the human auricular chondrocytes (hAUR)

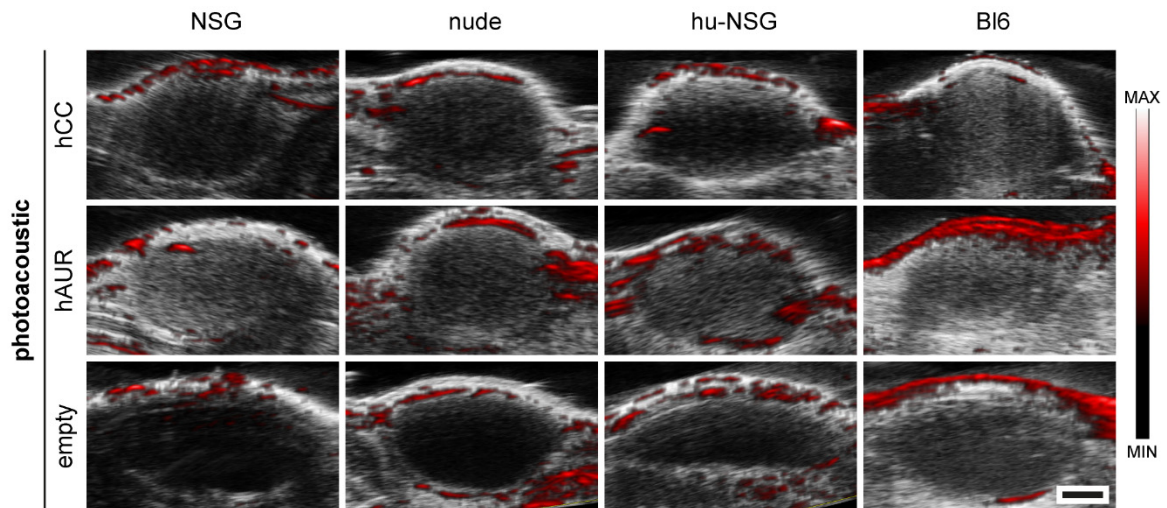
Human engraftment donor for hu-NSG (female)					
A*01:01	A*30:02	B*08:01	B*08:01	C*07:01	C*07:01
DRB1*03:01	DRB1*03:01	DRB3*01:01	DRB3*02:02		
DQB1*02:01	DQB1*02:01	DQA1*05:01	DQA1*05:01		
DPB1*01:01	DPB1*130:01	DPA1*01:03	DPA1*02:01		

hCC (male)					
A*03	A*30	B*35	B*55	C*03	C*04
DRB1*12	DRB1*14	DRB3*02			
DQB1*03	DQB1*05	DQA1*01	DQA1*05		
DPB1*02	DPB1*04	DPA1*01	DPA1*01		

hAUR (male)					
A*01	A*26	B*18	B*38	C*07	C*12
DRB1*04	DRB1*11	DRB3*02	DRB4*01		
DQB1*03	DQB1*03	DQA1*03	DQA1*05		
DPB1*04	DPB1*04	DPA1*01	DPA1*01		

771

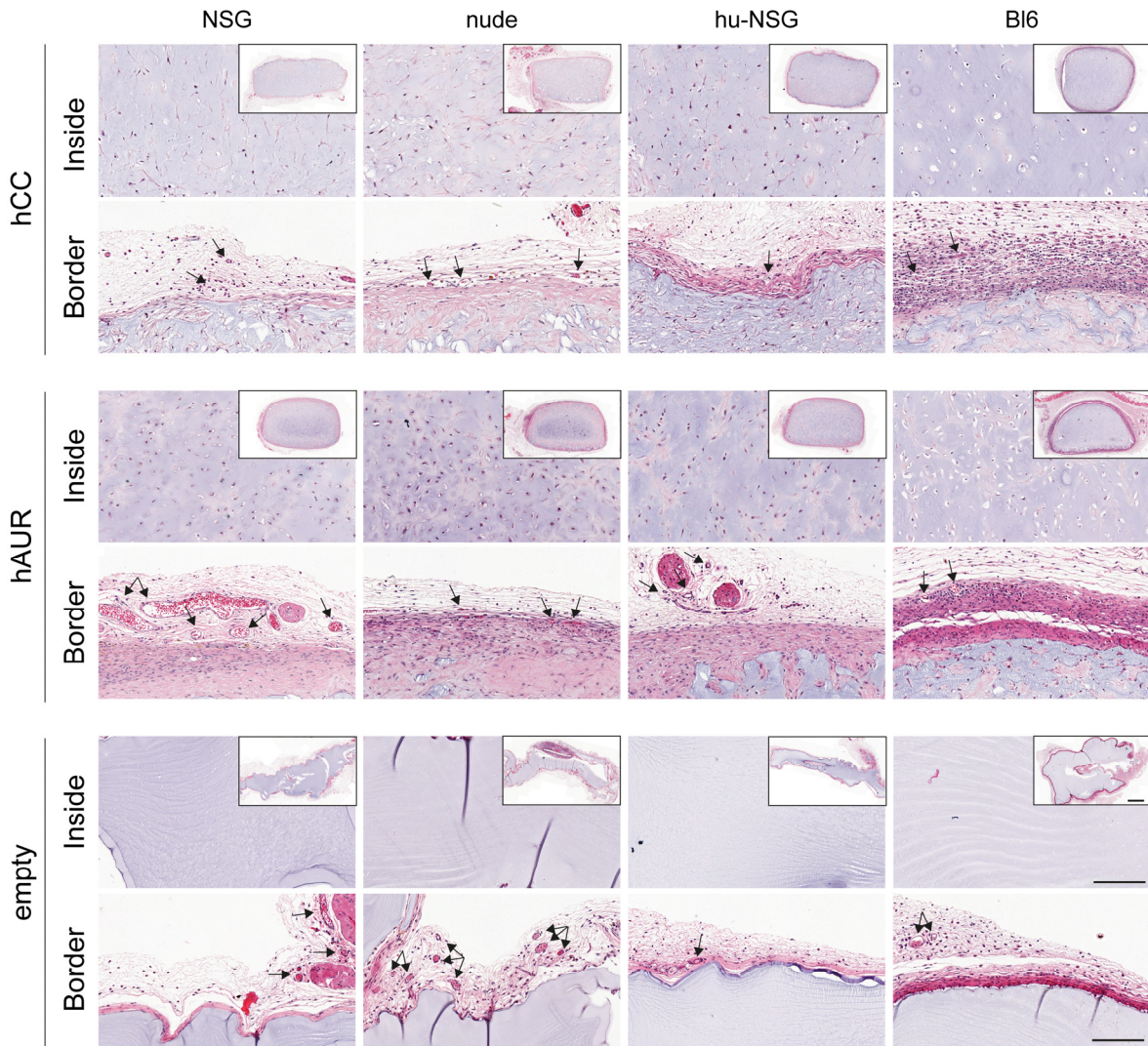
772



773

774 *Supplementary Figure 1 Photoacoustic images of HA-TG constructs at 4 weeks after implantation. Photoacoustic images*
 775 *are depicted as overlay of ultrasound and heat map of oxyhemoglobin saturation ($\lambda=700\text{nm}$). Scale bar: 1mm.*

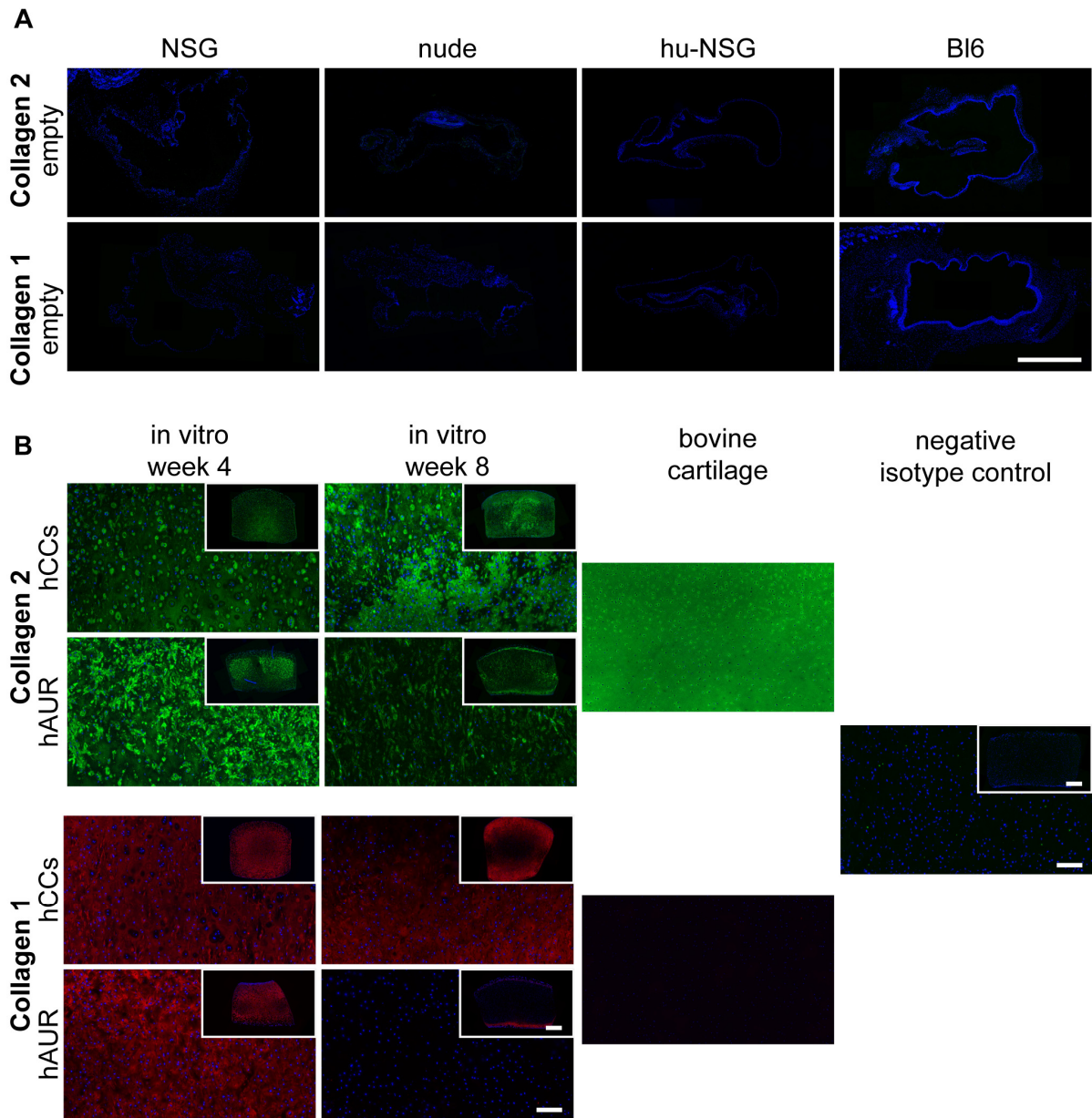
776



777

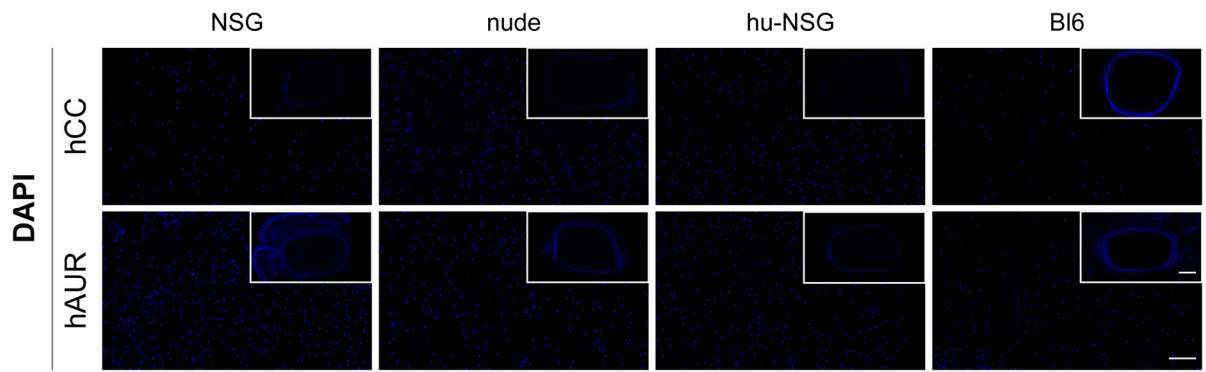
778 *Supplementary Figure 2 Hematoxylin and eosin (H&E) staining of HA-TG hydrogels after 4 weeks of in vitro preculture and*
 779 *4 additional weeks in vivo. Representative images of hydrogel inner region (inside) and outer border with fibrous capsule*
 780 *(border). Arrows point to visible blood vessels. Scale bar close up: 500µm, scale bar insert: 100µm.*

781



782

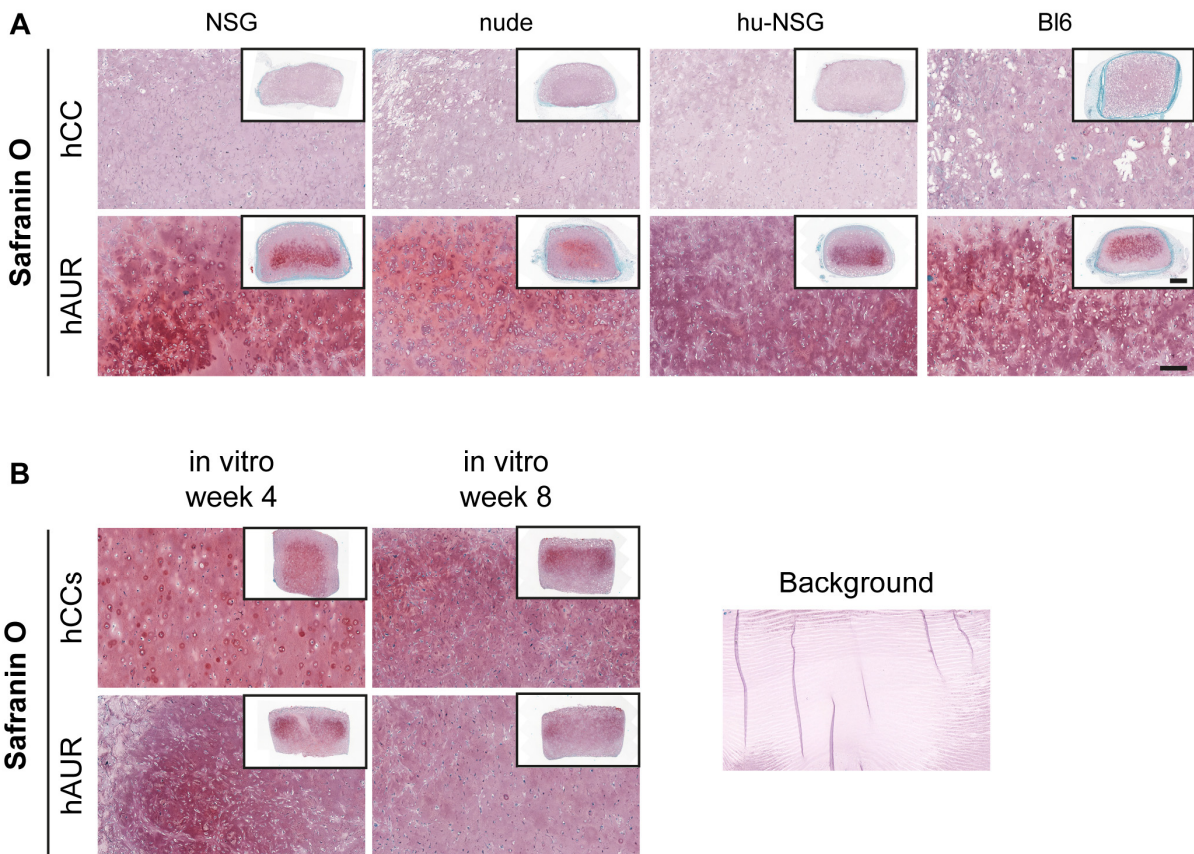
783 *Supplementary Figure 3 A: Collagen 2 and 1 immunohistochemical staining of acellular HA-TG hydrogels after 4 weeks of*
 784 *in vitro preculture and 4 additional weeks in vivo. B: Collagen 2 and 1 staining of HA-TG hydrogels after 4 and 8 weeks in*
 785 *vitro and HA-TG background staining. Bovine cartilage and IgG isotype antibody were used as controls. Scale bar close up:*
 786 *500µm, scale bar insert: 100µm.*



787

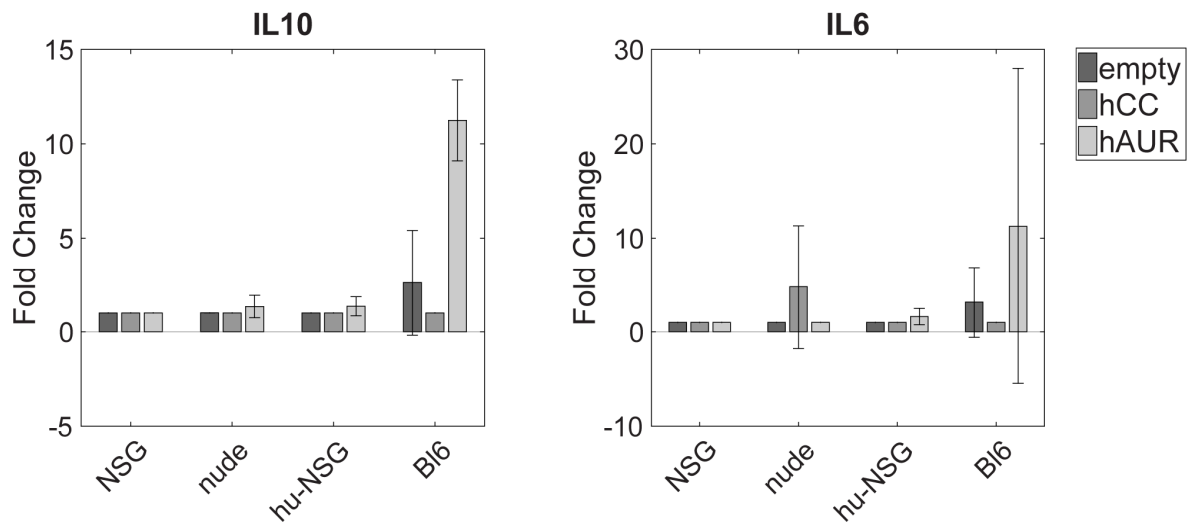
788 *Supplementary Figure 4 DAPI staining of HA-TG hydrogels after 4 weeks of in vitro preculture and 4 additional weeks in*
 789 *vivo. Scale bar close up: 500µm, scale bar insert: 100µm.*

790



791

792 *Supplementary Figure 5 A: Safranin O staining of HA-TG hydrogels after 4 weeks of in vitro preculture and 4 additional*
 793 *weeks in vivo. B: Safranin O staining of HA-TG hydrogels after 4 and 8 weeks in vitro and HA-TG background staining. Scale*
 794 *bar close up: 500µm, scale bar insert: 100µm.*



795

796 *Supplementary Figure 6 Inflammation markers IL6 and IL10 detected in mouse serum and normalized to baseline values*
 797 *acquired 10 days before surgery. Values below the limit of detection were set to the corresponding lower limit of detection.*
 798 *IL1- β , IL4 and TNF- α values were below the limit of detection of the assay.*

799

800 *Table 3 Baseline values of C-reactive protein (CRP), serum amyloid A (SAA) and serum amyloid protein (SAP) prior to*
 801 *experiment*

	NSG	nude	hu-NSG	Bl6
CRP (pg/ml)	5104.8	11895.5	10451.6	6062.5
SAA (pg/ml)	961.0	5509.1	2217.4	881.2
SAP (pg/ml)	90286.5	71014.9	61907.2	3662.9

802

803